Residual Cube Strength and Microstructural Properties of Fire-Damaged Biofibrous Concrete with GEP-Based Prediction Model

Oluwatobi Gbenga Aluko[1,2] · Jamaludin Mohamad Yatim[1] · Mariyana Aida Ab. Kadir[1,3] · Khairulzan Yahya[1]

Abstract

Concrete under thermal loads is characterised by cracking and pore pressure build-up resulting in spalling and deterioration. Its retained strength is crucial to structural soundness and serviceability. Past findings indicate that some fibres could mitigate crack propagation and pore pressure in heated concrete. However, kenaf fibre-reinforced concrete (KFRC) is yet to be studied. This research presents an experimental report on kenaf fibre normal strength concrete (KFNSC) (grade 40), using an optimum volume (0.75%) and length (25 mm), heated from 100 to 800 °C, sustained for 1, 2, and 3 h, and tested after cooling. The microstructure and thermal properties of treated fibre were examined using scanning electron microscope and thermogravimetry analysis. The residual compressive strength, microstructure, weight loss, and ultrasonic pulse velocity of KFRC were determined and compared with non-fibrous specimens. The test results revealed that KFNSC climaxed its compressive strength at 300 °C and was thermally stable up to 400 °C, compared with Plain normal strength concrete, with superior performance. However, both strengths declined, and the microstructure worsened with increased temperature and exposure duration. A Gene Expression Programming model was developed for prediction and gave a perfect correlation with empirical data. The research would offer technical information for biocomposite standards development and application strategy.

Keywords Biofibrous concrete · Biofibre · Residual strength properties · Kenaf fibre · Elevated temperature · Gene Expression Programming

1 Introduction

Fibres are incorporated into concrete to achieve specific roles under severe conditions, such as elevated temperatures [1]. The high manufacturing cost of conventional fibres and the need for greener biomaterials have led to the adoption of plant-based fibres in concrete. Substantial research efforts are currently exerted due to their relatively high stiffness, low processing energy, and CO_2 neutrality [2]. Biofibres obtained from cotton, hemp, jute, bamboo, flax, ramie, coconut, sisal, bagasse, and kenaf plants [3, 4] have been included in the concrete for over 40 years with significant properties improvement, with more research opportunities [5–7]. Despite the inherent merits of biofibres, they often exhibit weak fibre–matrix affinity and water absorption issues that affect composite properties [3]. They are controlled through fibre alkaline treatment, the most typical method to improve interfacial properties [3]. In addition, biofibres performance is influenced by type and selection, harvest time, processing and modification method, volume, and orientation and distribution within the matrix [4]. One of the critical parameters in structural design for serviceability requirements is fire resistance. It is the ability to build elements to display some restraints to fire and function as load-bearing elements under fire exposure [5, 6].

Many existing studies have revealed the performance of conventional fibres (steel, synthetic, hybrid) in concrete exposed to elevated temperatures through a crack and vapour pressure mitigation. Polypropylene (PP) is the common type of synthetic fibre, and steel has been used in high-strength concrete exposed to high thermal loads [7–10]. It

✉ Oluwatobi Gbenga Aluko
aluko1977@graduate.utm.my

1 School of Civil Engineering, Universiti Teknologi Malaysia, 81310 Skudai, Johor, Malaysia

2 Department of Civil Engineering, Ekiti State University, Ado Ekiti, Nigeria

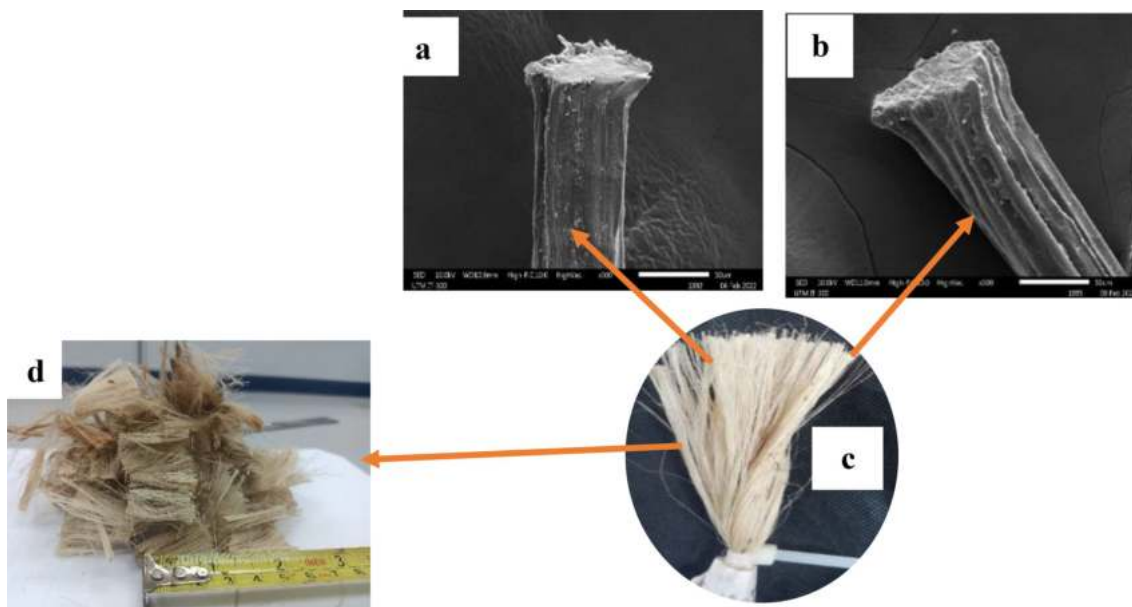3 Institute of Noise and Vibration, Universiti Teknologi Malaysia, Skudai, Malaysia

🖄 Springer

Fig. 1 **a** SEM of untreated kenaf fibre; **b** SEM of treated kenaf fibre; **c** Kenaf fibre macroimage; and **d** short-discrete kenaf fibre

also includes a steel and synthetic fibre hybrid in heated concrete [11, 12]. However, there is still a lack of studies on the effect of biofibres on concrete bared to fire or extreme temperatures. Ozawa et al. [13] reported the effect of jute fibre (vol:0.075%, Length: 12 mm) on heated high-performance concrete with a temperature of up to 500 °C under a stressed testing method. The concrete properties declined as the temperature rose, concluding that jute fibre deterred spalling in heated high-performance concrete (HPC) compared to the reference samples. Moreover, Zhang et al. [14] studied the effect of jute fibre's water absorption properties as it lessens heated ultra-high-performance concrete spalling. Grubeša et al. [15] also studied how hemp fibre could reduce the crack extension of thermally loaded concrete. Juradin et al. [16] reported the superior residual properties of concrete reinforced with Spanish broom fibres compared to polypropylene fibre. Mihoub et al. [17] examined the high-temperature impact on concrete reinforced with Alfa fibre and concluded that the composite could be used for sustainable concrete, with acceptable residual properties comparable with polypropylene composite. These findings show that biofibre could improve some degrading consequences of fire in concrete. Nevertheless, many of these investigations concentrated on high-strength and ultra-high-strength concrete, with minimal reports on normal-strength concrete. To date, there has been no report on residual cube and microstructural properties of KFRC with varying temperatures and exposure durations in a combined investigation. Furthermore, compressive strength and microstructures are essential to the post-fire properties of concrete because they are parameters

that could be used to evaluate strength loss and worsening conditions of concrete materials [1, 18]. However, the physical and mechanical characteristics often receive more attention than the microstructure, which is the part of the concrete capable of unveiling the coarsening process of the fire-damaged transition zone and the roles of fibres, aggregates, and cement paste in the heated matrices.

The kenaf plant has advantages over other crops because of its short plantation cycle, flexible environmental demands, high yield, tensile strength property, low density, high aspect ratio, and modulus [4]. Notably, the kenaf fibre is available locally and obtained from the kenaf plant, similar to cotton [4]. It is grown in large quantities and commercially in Malaysia for biocomposite product development. The processing cycle of kenaf fibre usable in concrete is shown in Fig. 1. Kenaf fibre-reinforced concrete has been researched for fibre characterisation, composite development, and structural applications, including marine structures [4, 19–22], with significant findings on its performance. However, its performance under elevated temperatures is the current focus considering the present attention on biofibrous concrete due to improved properties displayed at ambient temperatures and unforeseen fire incidence risk.

Understanding the characteristics of concrete post-fire has led researchers to embrace diverse numerical methods for an easy and rapid solution which has attracted attention lately [23]. Thus, the empirical results were used to develop a prediction model using Gene Expression Programming (GEP). Candida Ferreira developed the GEP software as a machine learning tool to incorporate simple linear chromo-

Table 1 Properties of alkaline-treated kenaf fibres

Fibre	length (mm)	Diameter (μm)	Ave. aspect ratio	Density (Kg/m^3)	Tensile strength (MPa)	Elastic Modulus (GPa)	Elongation at yield (%)
	25	40.1–115.2	500 μm	1.05–1.52	136–930	15–54	1.6–1.77

somes of fixed length to encode simple linear chromosomes of fixed size (genotype) to process datasets for model development [24, 25]. The GEP software is advantageous because regression algorithms operate on the premise of predefined functions, with subsequent regression analyses of these functions. Additionally, the GEP approach adds or removes different combinations of parameters to be considered for an expression that most suits the experimental findings instead of defining a predefined function. [26, 27]. Therefore, chromosomes and expression trees (ETs) are the two primary components of GEP. GEP employs the genetic code and the ETs language, allowing precise phenotypic inference from the sequence of genes and, inversely, known as the Karva language [26]. Several researchers have adopted GEP to predict the post-fire properties of concrete. Tanyildizi et al. 2010 [26] modelled the mechanical characteristics of lightweight concrete having silica fume bared to high temperatures using GEP. In addition, Ashteyat et al. 2020 [25] reported the compressive strength of lightweight short columns exposed to elevated temperatures. The authors discovered that GEP models are robust to predict the strength reduction factor of the lightweight column. This finding is similar to the study by Nematzadeh et al. 2021 [28], which observed good precision in the developed genetic programming-based equations comparable to experimental results.

Therefore, the increasing quest for greener construction materials must be balanced with concern for their fire endurance. This study presents assessment reports of the residual compressive and morphological characteristics of KFNSC with varying temperature and exposure duration, including weight loss, UPV, and the significance of kenaf fibre in the matrix regarding failure mood and post-cracking mechanism compared to plain concrete. This research offers a performance yardstick comparable with other fibres, steel, synthetic, or biofibres regarding fibre-reinforced high-temperature performance.

2 Materials and Methods

2.1 Material

Aggregates, cement, kenaf fibre, potable water, and superplasticiser were used for this research. However, kenaf fibres require modification before using them in the concrete mixture (Table 1).

2.1.1 Fibre Alkaline Treatment and Properties

The kenaf fibre used in this research was obtained from the National Tobacco Board at Kelantan, Malaysia. Cellulosic fibres are hydrophilic and require modifications to improve strength and fibre–matrix bond. The improvement of kenaf fibre is made using NaOH, which contains functional groups that can bond with the hydroxyl group of the biofibres [29]. Based on earlier studies on kenaf fibre treatment, the optimum alkaline concentration is 5% NaOH [30]. The process cycle in Fig. 2d & e shows a picture of treated and dried kenaf fibre. The fibres were tied into bunches, combed into strand-likes (Fig. 2f), cut into 25 mm as short-discrete fibre, and added to the concrete matrix. Previous studies from the same laboratory optimised kenaf fibre usage in concrete and ascertained 0.75% and 25 mm as the optimum volume and length [31, 32]. The physical and strength characteristics of the kenaf fibre used in this study were obtained through laboratory tests [33].

2.1.2 Fibre Morphology and Thermogravimetric Analysis

The alkaline treated and untreated kenaf fibres morphology was observed under a Variable-Pressure Scanning Electron Microscopy (VPSEM), JEOL JSM-IT300LV with a working voltage of 20 kV, at T03, Universiti Teknologi Malaysia, Johor Bahru. The impact of alkaline treatment on the fibre surface was observed using VPSEM. Figure 1a & b shows the micro- and macrographs of the treated and untreated kenaf fibre. From the micrographs of the treated fibre, the alkaline solution removed the wax and oil, protecting the outer face of the fibre cell wall. It also removed the hydrogen bonding in the interconnected structure of the fibre cellulose, hemicellulose, and lignin, thereby improving the fibre surface roughness and interfacial properties (Fig. 1b). The smooth surface of the untreated fibre shows the network of cellulose, wax, and oil covering the surface (Fig. 1a), as reported by Grubeša et al. [15] on hemp fibre modification. Figure 1d shows the chopped kenaf fibre to be used in concrete.

TGA was used to monitor the mass and substance of the kenaf fibre at varying high temperatures. It revealed the thermal degradation of treated and untreated kenaf fibre samples when exposed to a guided temperature treatment in a controlled environment, using TA instrument, TGA, and Q500 model, with a 10 °C/min heating rate. The sample size is 7.49 mg. From the TGA chart (Figs. 3 and 4), treated fibre
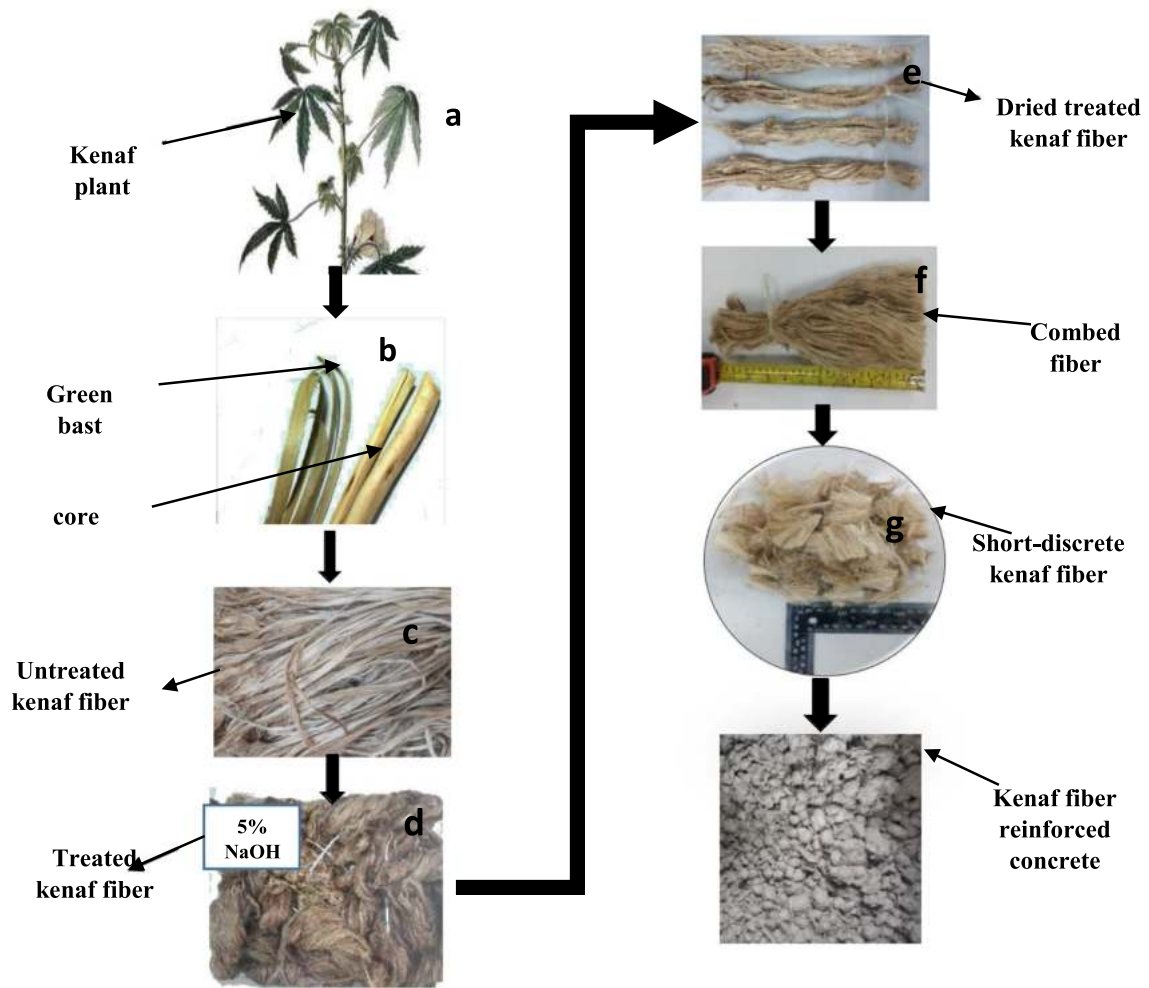
Fig. 2 Fibre preparation cycle: kenaf plant—short-discontinuous fibre (**a**-**g**)
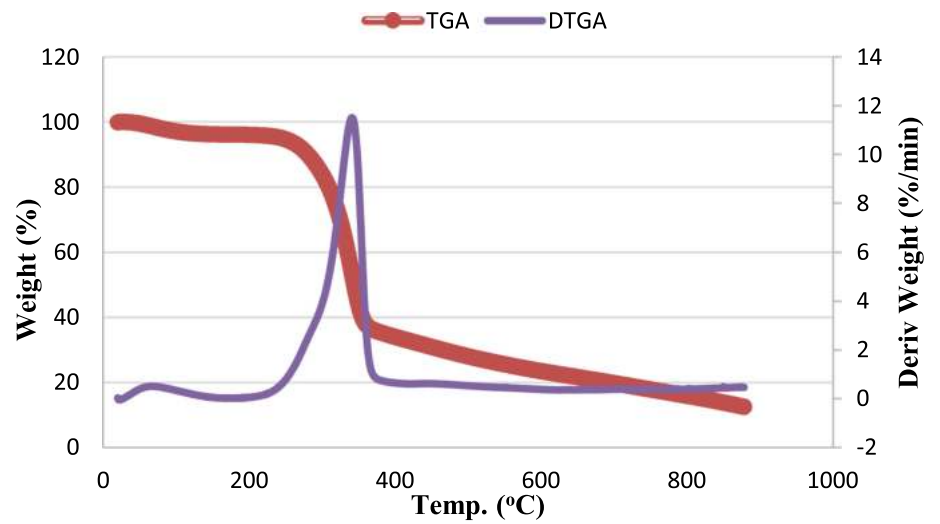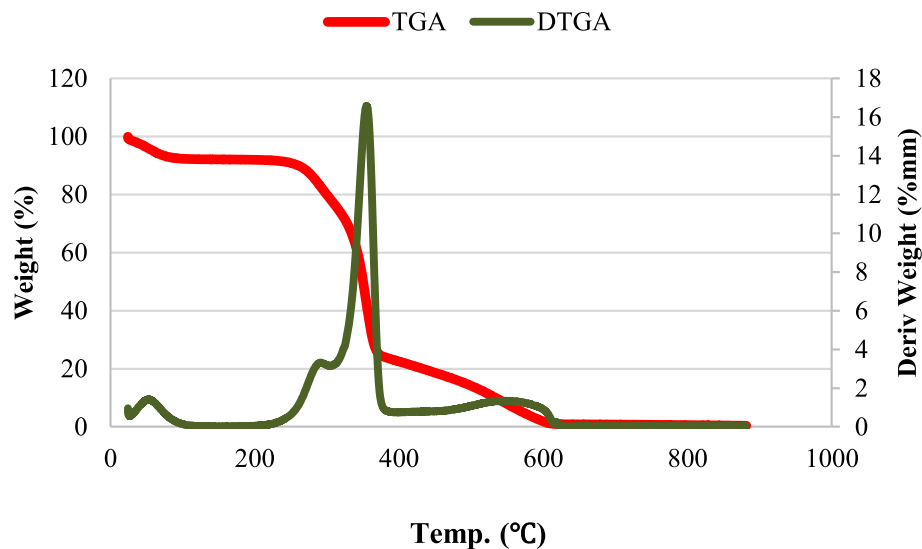
Fig. 3 TGA for treated kenaf fibre

Fig. 4 TGA for untreated kenaf fibres

had about 4.5% weight loss at 50 °C due to water removal, which was not noticeable in the treated kenaf fibre. This was unlike the untreated fibre, where there was substantial weight loss. The weight loss of kenaf for temperature span describes the decomposition and thermal stability of the kenaf fibre and examines the physicochemical nature of the fibre [34]. The treated fibre stabilised until 260 °C and lost 65% of its weight, caused by degeneration of lignin, breaking down of polymers and hemicelluloses, and pectin due to heat treatment. At 360 °C, treated fibre decomposed partially and completely at 700 °C with 100% weight loss. However, the untreated fibre decomposed partially at 360 °C with 75% weight loss and 600 °C with 100% weight loss. It has been established that treatment removes almost all the biopolymer layers from the fibre exterior, which lessens the deterioration temperature, as confirmed by the apparent weight loss [35]. Therefore, the treatment helps improve the thermal stability of the kenaf fibre.

2.1.3 Aggregate and Cement Properties

Sharp river sand was graded adequately as fine aggregate, with a maximum grain size of 4.75 [36]. Also, crushed granite of 10 mm sizes was used in the mix [36]. Ordinary Portland cement (OPC, 142.5) based on ASTM-C150 [37] was used for this study, and the chemical compound is shown in Table 2. This research used the Rheobuild 1100 brand of superplasticiser containing synthetic polymer and complied with ASTM C494. This was because kenaf fibres decrease the

workability of the concrete and may affect curing problems.

2.2 Method

2.2.1 Concrete Mix Design

This study used the Department of the Environment (DOE) mix design method (DOE-Method, 2013). Two mixes with 126 samples were made for the residual compressive strength test. The mix proportion is shown in Table 3.

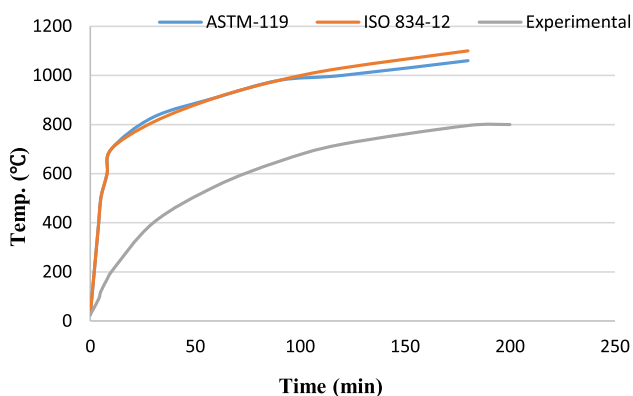#### 2.2.2 Concrete Sample Preparation

The mixing method used to prepare KFNSC samples was similar to plain concrete, except for including fibre. The chopped kenaf fibres were hydrated for 30 min before mixing [32]. Consecutively, the aggregates, cement, and water were poured into the mixer and adequately mixed, after which the short-discontinuous kenaf fibres were gradually dispersed into the matrix and mixed appropriately for 3 min. Dosages of superplasticiser were added and mixed for 5 min to ensure a uniform mixture. The slump and compaction factor test was done following BS EN 12350-2 2009 [38], and the concrete was placed in the oiled moulds and appropriately compacted on a vibrating table. The concrete samples were de-moulded after 24 h and cured for 28 days. The samples were allowed to dry before being weighed and tested for their UPV and compressive strength to obtain their values before thermal treatment.

Table 2 Cement chemical properties

Constituent	CaO	SiO$_2$	Al$_2$O$_3$	Fe$_2$2O$_3$	MgO	SO$_3$	Total Alkalis	Insoluble Residue	Loss of Ignition	Silica Modulus
Weight (%)	64.64	21.28	5.6	3.36	2.06	2.14	0.05	0.22	0.92	2.38

Table 3 Mix proportion for KFRC and control

Mix	KF(%)	KF(kg/m3)	Water (w/c = 0.47,0.33) (kg/m^3)	Cement (kg/m^3)	Fine agg. (kg/m^3)	Coarse agg. (kg/m^3)	Superplasticiser (1%)
PC	0	0	250	532	688	875	5.32
KFNSC	0.75	9	250	532	688	875	5.32

Fig. 5 Experimental heating curve versus standard curve (ISO 834–12 and ASTM E 119)

Fig. 6 Temperature–time heating curve for the experiment

2.2.3 Heating and Cooling of Concrete Samples

The standard fire test evaluates the resistance of structural elements to fire [35]. This research used the unstressed residual testing method in which the samples are heated and cooled to room temperature before strength tests [36]. From Fig. 5, the furnace thermal rating described as experimental is lower than ASTM-119 [35] and IS0834-12 [39]. However, the experimental heating curves indicated a similar behaviour to the standards. Furthermore, the lower heating rate benefits the specimens by avoiding 'too early' thermal strain and explosive spalling at the initial stage of the heating process, as RILEM [40] recommends and also confirmed by Li et al.(2021) [41]. However, some previous researchers have adopted this 'non-standard' for concrete assessment [42, 43]. Figure 6 depicts the heating cycles for each targeted temperature, such that 't' represents 1, 2, and 3 h. Figure 7a shows the electrically controlled muffle furnace containing a sample, while Fig. 7b shows KFRC cube samples to be heated from 26 °C to targeted elevated temperatures (100 °C, 200 °C, 300 °C, 400 °C, 600 °C, 800 °C). The initial heating rate of 15.2 °C/min for the 100 °C targeted temperature took 6.6 min,

and 800 °C at 4.1 °C/min took 195 min. The temperatures were sustained for 1, 2, and 3 h. Then, samples were allowed to cool naturally to ambient temperature within 24 h after heating. Phan et al. [44] reported that the time for a core of a concrete sample to cool down to an ambient temperature is roughly 20 h. Therefore, it is practicable to consider the cubes samples to have cooled to room temperature after 24 h. The samples were weighed to assess loss in weight and other physical characteristics before the UPV test, compressive strength, and microstructure assessment.

2.3 Assessments Performed on Heated Hardened Concrete

After ensuring the samples were cooled naturally, the samples were assessed to check the heated weight loss of the composites, UPV, and compressive strength characteristics.

Fig. 7 **a** Concrete samples inside the furnace, **b** unheated samples for heating
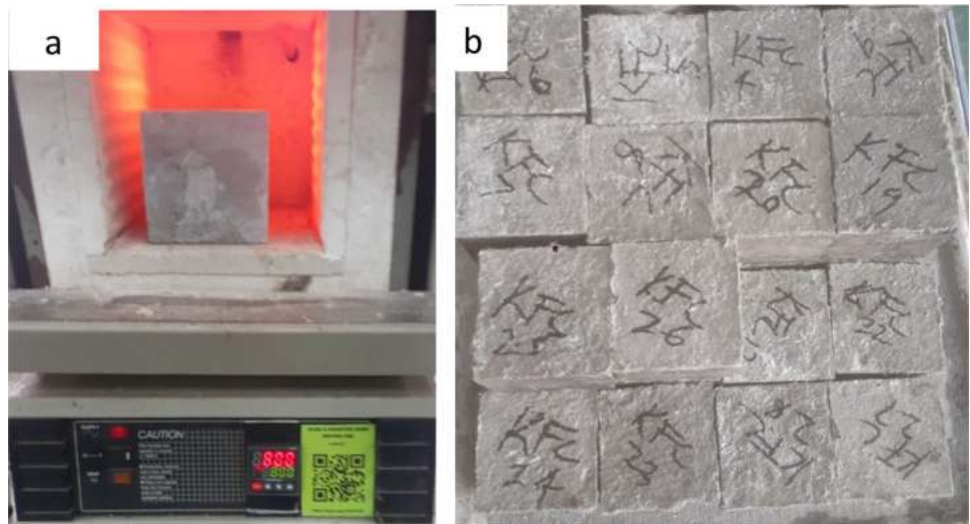
2.3.1 Weight Loss

For this study, each sample for each targeted temperature was weighed before and after heating on an electronic balance of ± 0.2 g to obtain the pre-heating weight (W_1) and post-heating weight (W_2). Percentage weight loss was determined using Eq. 1.

$$\text{Weight loss} = \left(\frac{W1 - W2}{W1}\right) \times 100 \tag{1}$$

2.3.2 Ultrasonic Pulse Velocity (UPV)

The UPV test estimates the structural integrity and uniformity of concrete samples without damaging the samples to assess cracks and pores in concrete. The test was performed using a Pundit7 tester, following BS 1881-203 (1983). The instrument measures the time an ultrasonic pulse travels within the concrete through two transducers to transmit and receive the pulse at both ends. Figure 8 shows the picture of the UPV tester used. Thus, the compressional wave pulse velocity 'V' of the samples before and after the heating was estimated using Eq. 2. The strength reduction factor was obtained by dividing the UPV values of the targeted temperature over the ambient temperature value (26 °C).

$$V = \frac{L}{T} \tag{2}$$

where; V is the pulse velocity in Km/sec., L is the distance in (mm), and T is the time, in (sec.) required for the pulse to travel through the distance.

Fig. 8 The UPV tester for the samples

2.3.3 Residual Compressive Strength

The high-temperature impact on the samples was evaluated by estimating the retained strength characteristics of concrete samples at varying temperature levels. The compressive strength test was undertaken by applying a 2500kN compression machine, with a loading rate of 6kN/s, on air-cooled, 100 mm cube KFRC samples for each targeted temperature, and the average values were recorded as the residual compressive strength [45]. The results were also presented

Fig. 9 Heated cube samples under compression loading

in relative residual strength/strength reduction factor as a function of temperature, which is a much better graph for analysing and comparing changes in strength properties. The strength reduction factor is the residual strength ratio at targeted temperatures to the ambient temperature strength. An example of cubes under crushing load is shown in Fig. 9.

2.3.4 Microstructure Assessment

Microstructure examination is necessary to grasp physio-chemical transformation within the ITZ fully. Therefore, small crumbs from the KFRC and control samples were obtained during testing for each targeted temperature for morphological evaluations using Variable-Pressure Scanning Electron Microscopy (VPSEM), JEOL JSM-IT300LV with a working voltage of 20 kV, at T03, Universiti Teknologi Malaysia, Johor Bahru, Malaysia. These micrographs were critically analysed to infer the reason, pattern, and extent of KFRC deterioration. Then, its effects on retained properties of KFRC were undertaken based on (ASTM-C1723-10, 2010).

2.3.5 GEP-Based Model

GeneXproTools 5.0 was used to build the GEP model for the current study. Therefore, chromosomes and expression trees (ETs) are the two primary components of GEP. The GEP employs the genes and language of the ETs [25], and the information is changed from chromosomes to ETs. The training and testing/validation data are used to run several GEP models. The formulations are based on training sets and are further tested by test set values to measure their generalisation capability. GEP parameters are shown in Table 4, and the limits of responses and predictors used are presented in Table 5. The data used in test/validation and training sets are randomly selected, allowing the system to partition 67% of the data sets

Table 4 The GEP setting parameter

Function Set	$+, *, -, \sqrt{}$
Genes	3
Chromosomes	30
Head size	7
Linking function	Addition
Mutation rate	0.00138
Inversion rate	0.00546
Transportation rate	0.00546
One-point recombination rate	0.00277
Two-point recombination rate	0.00277
Gene recombination rate	0.00277
Gene transportation	0.00277

Table 5 Limits of the predictors and responses used in the GEP Modelling

Predictors	Lower limit	Upper limit
Applied temp (°C)	26	800
Exposure duration (h)	1	3
Concrete grades (MPa)	40	40
Responses		
Compressive strength (MPa)	40.3	60.4

used for training, while 33% were used to test/validate the model. Different GEP models are created using various gene, chromosome, head size, and linking function configurations. A total of 212 models were generated in this research, but the model that best fits the experimental findings was chosen. The finest model that forecasts the residual compressive
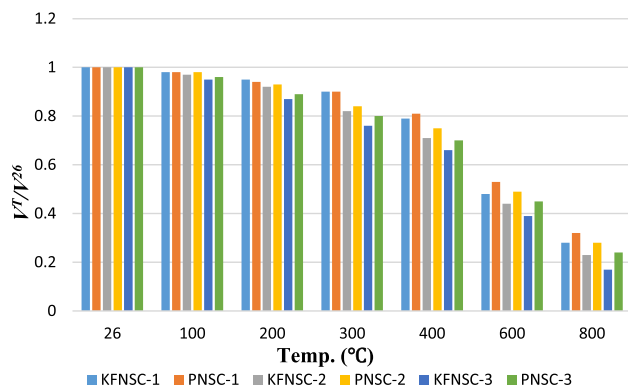
Fig. 10 Relative residual UPV for 1, 2, and 3 h exposure duration
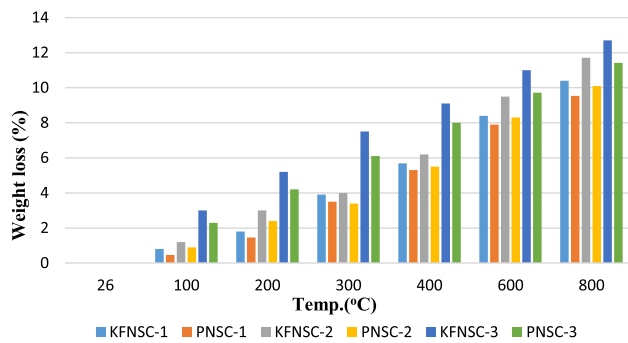

Fig. 11 Percentage of average cube weight loss with temperature variations for KFNSC for 1, 2, and 3 h

strength of KFNSC has been developed through many experiments. It was evaluated after being satisfied with the model's performance based on statistical fitness parameters like the coefficient of determination (R^2) and correlation coefficient. Additionally, the difference in error between the experimental and predicted was assessed through mean absolute error (MAE), root-mean-square error (RMSE), residual standard error (RSE), relative absolute error (RAE), and root relative squared error (RRSE). The model was extracted from the expression trees shown in Fig. 27 in equation form (Eq. 3), using d_0, d_1, and f_c, and Cs are numerical constants [25].

3 Results and Discussion

3.1 Properties of Heated Hardened Concrete

Table 6 shows the residual values for the UPV and compressive strength of samples for all elevated temperatures and duration. For identification purposes, KFNSC-1, KFNSC-2, KFNSC-3, PNSC-1, PNSC-2, and PNSC-3 represent 1, 2, and 3 h of the exposure period, as shown in Figs. 9, 10 & 11. This section presents and discusses the residual UPV values,

weight loss, compressive strength, and microstructure for 1, 2, and 3 h temperature durations for KFNSC.

3.2 High-Temperature Effect on Concrete UPV Values

An average residual UPV test result from elevated temperature and exposure period is presented in Table 6, and the reduction factor is presented in Fig. 10. Non-destructive testing (NDT) equipment was used to assess the quality of KFNSC at the residual testing condition. The exposure period was observed to have a remarkable influence on the results. Kenaf fibre reduced the concrete densities of the KFNSC samples and made the UPV value lesser than PNSC. The UPV values of both concrete mixtures were high at room temperatures, while lower results were obtained at higher temperatures.

For 1-h exposure (Fig. 10), the UPV results for KFNSC and PNSC were 4.751 m/s and 4.856 m/s at ambient temperature, respectively, with PNSC having a higher value of 2.2%, depicting good concrete quality [46]. There was a gradual change in both samples before 400 °C. However, at 400 °C and above, the UPV result for KNSC and PNSC notably dropped. At 800 °C, KFNSC and PNSC retained 28% and 32% of ambient UPV values, respectively. For a 2-h exposure duration (Fig. 10), KFNSC UPV rapidly declined compared with PNSC, while at 800ºC, KFNSC and PNSC could only retain 23% and 28% of the value at ambient. For the 3-h duration (Fig. 10), the impact of exposure temperatures and duration was felt by both samples. This was seen in the rapid decline of the UPV values. KFNSC and PNSC could retain only 17% and 24% of their ambient value, respectively. The decline in the UPV result could not be entirely due to the decomposition of fibres, forming more porous interconnectivity within the composite. The impact of extreme temperatures on the worsening of concrete microstructure is valid for both fibrous and non-fibrous concrete. Zheng et al. and Awal et al. [47, 48] reported that the deformation of C-S-H at 450 °C and above made the concrete more porous, consequently diminishing the UPV values of the concrete samples and making the concrete more porous. This is similar to the report of Mohammadhosseini and Yatim [49] on UPV deterioration due to extreme temperatures.

3.3 The Effect on Concrete Weight

Figure 11 reveals the effect of elevated temperature and exposure period on the cubed weight of KFNSC compared to PNSC. One quick way of assessing concrete property at high temperatures is weight loss [50]. It has been established that weight loss in concrete increases with temperature increase. At high temperatures, weight loss in the concrete is due to the release of bound water from the cement paste and concrete porosity [51]. In addition, removing chunks of concrete

Table 6 Residual compressive strength and UPV for all temperature levels and durations

Properties	Mix-Temp. Duration	Temp. (°C)						
		26 °C	100 °C	200 °C	300 °C	400 °C	600 °C	800 °C
UPV	KFNSC-1	4.751	4.676	4.498	4.274	3.751	2.287	1.310
	KFNSC-2	4.751	4.624	4.385	3.891	3.386	2.102	1.000
	KFNSC-3	4.751	4.511	4.212	3.627	3.121	1.841	0.801
	PNSC-1	4.856	4.778	4.587	4.376	3.912	2.584	1.536
	PNSC-2	4.856	4.773	4.525	4.082	3.649	2.364	1.361
	PNSC-3	4.856	4.651	4.331	3.891	3.398	2.164	1.154
Compressive strength (MPa)	KFNSC-1	40.3	42.6	38.6	41.5	42.1	23.20	11.20
	KFNSC-2	40.3	42.3	38.2	41.0	39.7	21.20	9.100
	KFNSC-3	40.3	43.3	38.2	40.1	35.2	19.50	8.200
	PNSC-1	48.5	50.2	43.7	46.6	49.3	30.30	16.40
	PNSC-2	48.5	50.2	43.3	48.4	47.2	29.20	14.30
	PNSC-3	48.3	50.1	43.2	47.4	41.6	25.40	12.20

from the surface layers and strength loss are crucial reasons for weight loss [52] due to changes in stiffness and mechanical properties of the concrete at extreme temperatures [53]. Adding the kenaf fibre to the mix indicates sharing the mortar with the 'owner' aggregates. This means replacing cement paste with another lighter fibre in the mixture. Thus, the presence of kenaf fibre in concrete lessened the complete and expected reaction between water and cement particles to provide calcium-silicate-hydrate (C-S-H) gel and calcium hydroxide. This gel will possibly fill pores in the samples and increase the weight of each sample. At ambient, KFNSC samples had a lesser weight compared with PNSC. However, the samples were still within the acceptable weight for standard concrete.

For the 1-h duration, until 200 °C, there were no notable weight loss differences between both mixes (Fig. 11), which could be linked to removing water from the samples. At 400 °C, KFNSC and PNSC lost 5.7% and 5.3%, respectively. From 600 to 800 °C, KFNSC lost its weight drastically at 8.4–10.2% compared to PNSC with 7.9–9.53%. Also, for a 2-h duration (Fig. 11), both mixes have begun to experience weight loss faster. Between 600 and 800 °C, KFNSC had lost 9.5–11.7%, 1.6% higher than PNSC weight loss of 8.3–10.1%. From Fig. 11, weight loss at the 3-h duration became substantial between 600 and 800 °C, and KFNSC lost 11–12.7% of its weight, whereas PNSC lost 9.71–11.42%. At this point, both samples have experienced complete decomposition of the kenaf fibre, and the dehydration of cement paste and aggregates has worsened. Apart from the fibre deterioration in KFNSC, matrices with lower density and permeability tend to experience dehydration faster than samples with higher density, causing significant weight loss. Weight loss at higher temperatures could be ascribed to the loss of

binding capability of cement paste due to dehydration of C-S-H formation and breaking down of $Ca(OH)_2$. As a result, this leads to a loss of concrete stiffness and strength characteristics. This finding agrees with the report by Grubeša et al. [15], where hemp fibre was used. Weight loss at higher temperatures could be ascribed to the loss of binding capability of cement paste due to dehydration of C-S-H formation and breaking down of $Ca(OH)_2$, leading to loss of concrete stiffness and strength characteristics. Weight loss is related to the strength of concrete; as such, when the weight loss is more than 30%, almost 90% of the strength is lost [54].

3.4 Effect on Residual Compressive Strength

Compressive strength remains the most crucial property of concrete bared to extreme temperatures because it influences concrete performance diversely due to different material compositions and temperature variations [6]. The relative retained strength at a given temperature represents the residual strength ratio at various target temperatures to the strength at room temperature (26 °C). This indicates the strength degradation of the concrete samples as a function of temperature variation. Therefore, relative residual strength is a much better parameter for analysing and comparing changes in strength values. The average residual cube strength for 28-day KFNSC as a function of temperature and exposure duration is presented in Fig. 12. Furthermore, Fig. 12 shows compressive strength reduction factors for KFNSC for 1, 2, and 3 exposure hours. The effect of the kenaf fibre in a concrete composite is never significant in compressive strength improvement, even at ambient temperature. Therefore, strength improvement was not anticipated except for the
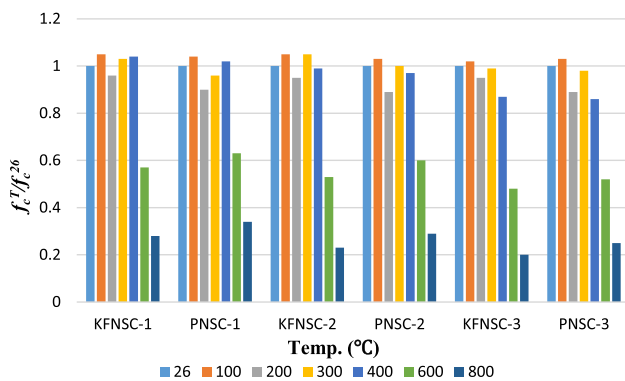
Fig. 12 Relative residual strength for KFNSC against temperature for 1, 2, and 3 h

regular concrete strength improvement initiated by physio-chemical responses to a specific extreme temperature level.

For 1-h exposure, KFNSC and PNSC strength improved by 5% and 4% at 100 °C, respectively, agreeing with Afshoon et al. (2020) [55]. The reason is not far-fetched as the dehydration of the samples at a lower temperature range creates van der Waals force, consequently increasing the strength. The marginal increase in compressive strength could also be accredited to the quickening of the release of chemically bound free water, exuding calcium hydro-silicate (CSH) and $(Ca(OH)_2$. However, the KFNSC and PNSC strengths were reduced at 200 °C by 4% and 1%, respectively. This could be credited to water loss from the samples, resulting in voids formation, thus a decline in the residual compressive strength and increasing the concrete permeability [56]. This occurrence is called a 'strength recession' [57]. At 300 °C, KFNSC had its peak strength. This could be due to the completion of the hydration phase, with vaporised water moving across the pores and voids of un-hydrated cement. This forms stronger bonds within the KFNSC matrix. However, PNSC is unable to recover completely at this temperature. Also, KFNSC and PNSC gained 2% and 4% strength at 400 °C and retained 28% and 34% of their ambient temperature strength, respectively.

For a 2-h duration (Fig. 12), the KFNSC gained 5% strength at 100 °C and 300 °C, respectively, while PNSC gained 3% and recovered fully at 300 °C. At 400 °C, the compressive strength declined sharply, with 23% and 30% strength retention for KFNSC and PNSC, respectively. Also, for 3 h (Fig. 12), KFNSC and PNSC only gained 2% and 3% at 100 °C, after which rapid strength degradation commenced. However, KFNSC and PNSC retained 20% and 25% at 800°C. Mohamedbhai et al. al (1986)[58] reported a similar result. Strength shoot-up for PNSC could be attributed to forming additional hydration products by converting the C–S–H state into a pectolite state [$NaCa_2Si_3O_8(OH)$]. About 100% of the strength was retained until 400 °C for both mixes. The KFNSC climaxed its strength with stability between 200 and 400 °C, which agrees with Ma et al. (2015)[59].

Between 400 and 600 °C, an acute loss was noticed from 600 to 800 °C for both mixes. Figure 12 shows the failure of the cube samples after crushing, and satisfactory failure was observed between 600 and 800 °C. At 600 °C, 50% and 40% of the KFNSC and PNSC strength were lost because 600 °C began aggregate deterioration [60]. Moreover, a progressive decomposition of C-S-H and portlandite resulted in crack formation. A similar strength loss was experienced at 800 °C for both mixes, the second stage of the C-S-H breaking up and generation of β-C2S [1, 61]. Therefore, it could be concluded that strength loss in KFNSC is a combined result of fibre and concrete deterioration [14]. Figure 13 shows the residual condition after crushing.

3.5 Effects on KFNSC Microstructures

This section analyses and presents the effects of the kenaf fibre and temperature exposure duration on the KFNSC microstructures.

3.5.1 Micrographs of KFNSC at Ambient Temperature

The results of unheated samples for both mixes were presented, discussed, and compared with the heated samples, as shown in Fig. 14a-d.

From Fig. 14a, b, c, & d, the micrograph of KFNSC and PNSC depicts an undamaged matrix at ambient temperatures, with ettringite and C-S-H formations. Also, Fig. 14a shows the fibre, while Fig. 14c shows a micrograph with a hole where the fibre has been pulled out. At this temperature, all the mechanical properties are still intact and undegraded. Figure 14a shows how the kenaf fibre reinforced the composite, functioning as bridges across cracks and pores at ambient temperature. It also showed that C-S-H gel formations spread across both matrices (Fig. 14b, c, & d). Both were matrices without microcracks or pores, showing how the fibres are firmly enfolded by C-S-H gel, indicating the existence of a strong bond between the kenaf and cement paste, as shown in Fig. 14a. The SEM image shows that fibre has good interfacial bonding with the cement paste, leading to small cracks along the fibre surface.

3.5.2 KFNSC Micrographs for 1-Hour Temperature Exposure

Figures 15, 16, & 17 reveal the effects of elevated temperatures on the KFNSC microstructure for 1 h and the role of kenaf fibres within the matrix compared with the control samples.

At 400 °C for 1-h exposure, the kenaf fibre within the matrix has not deteriorated entirely and is still active (Fig. 15a) and thus offered a bridging mechanism and cracked mitigation within the matrix. No cracks were observed on both matrices at this exposure temperature and duration.
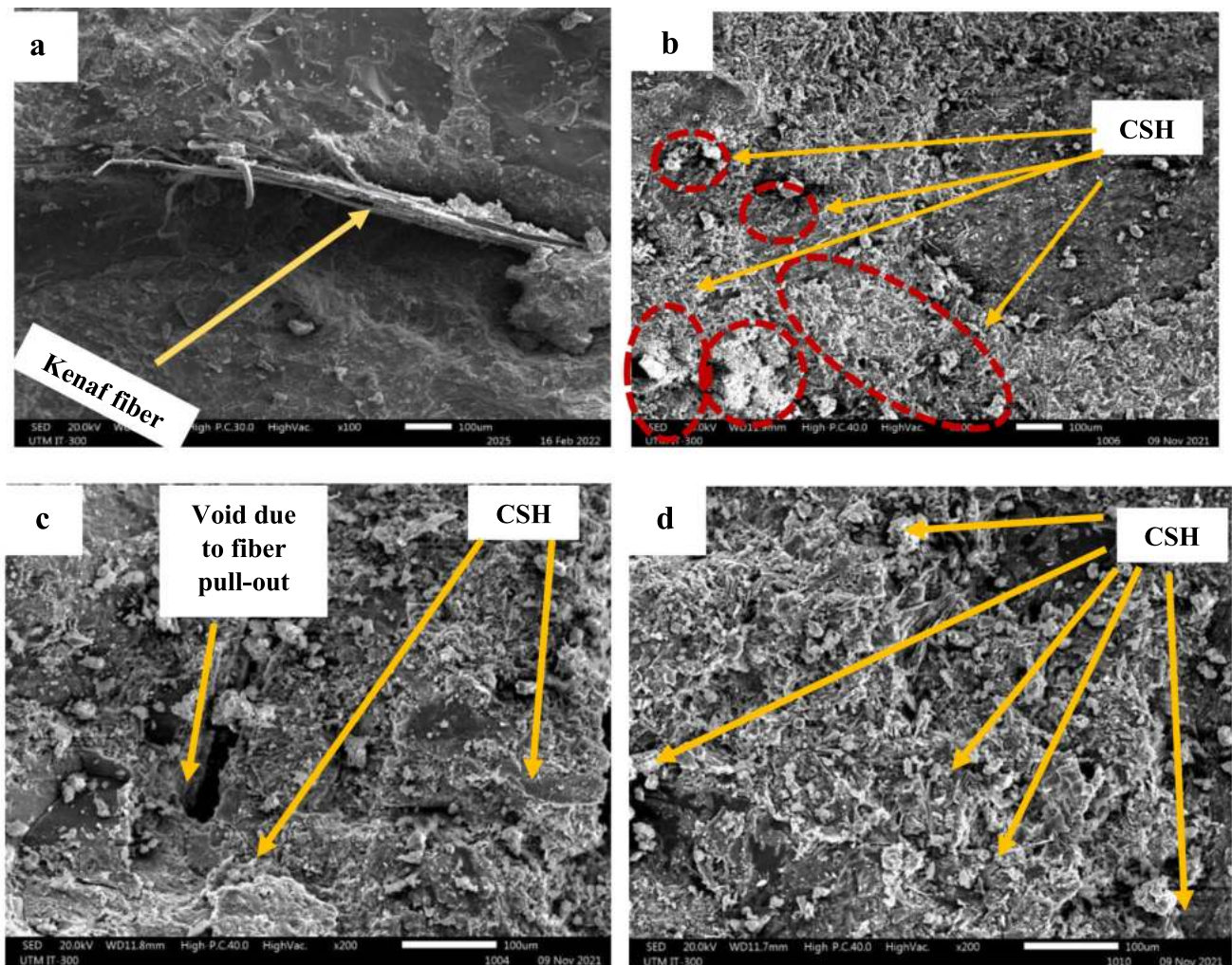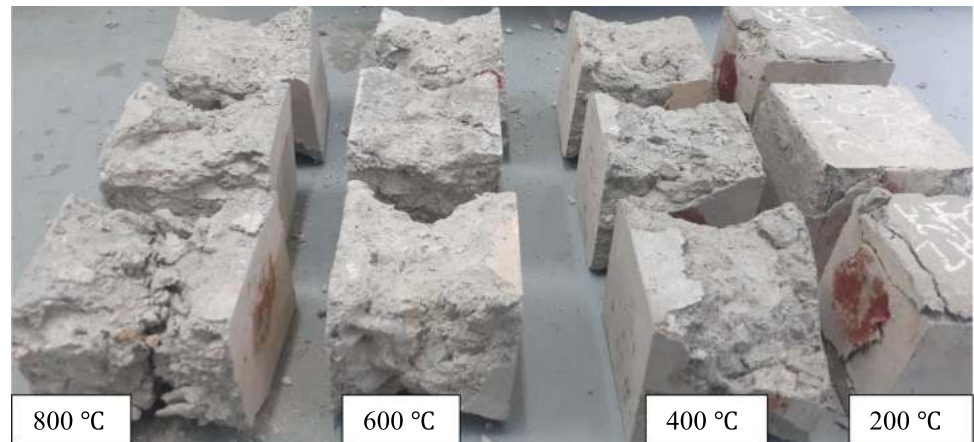
Fig. 13 Cube samples after crushing

Fig. 14 **a** and **c** KFNSC at 26 °C, **b** and **d** PNSC at 26 °C
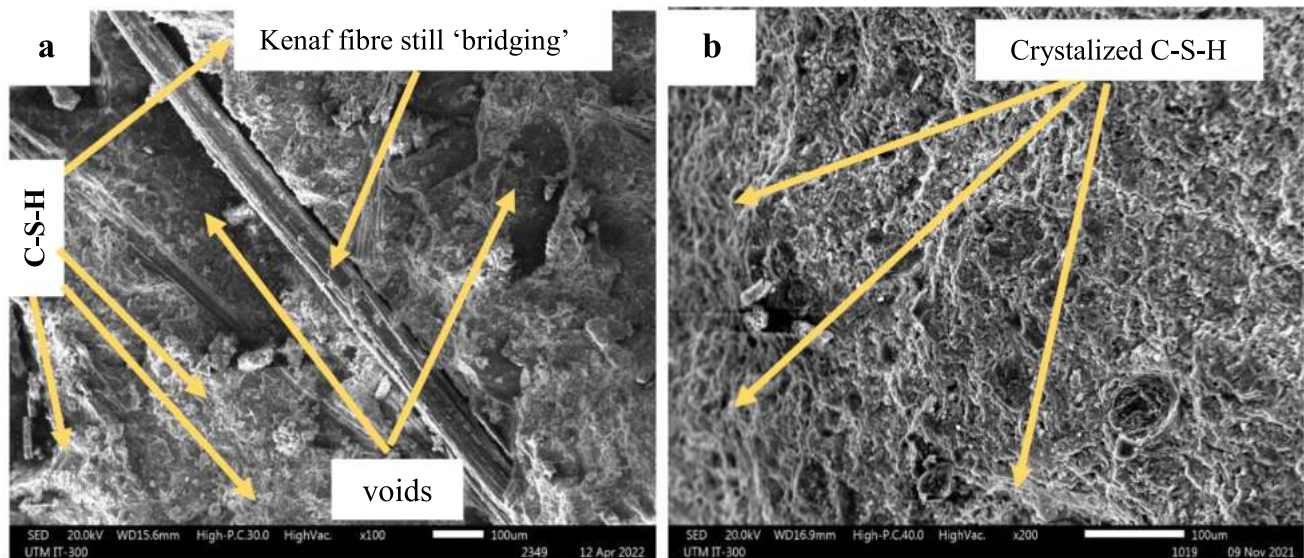
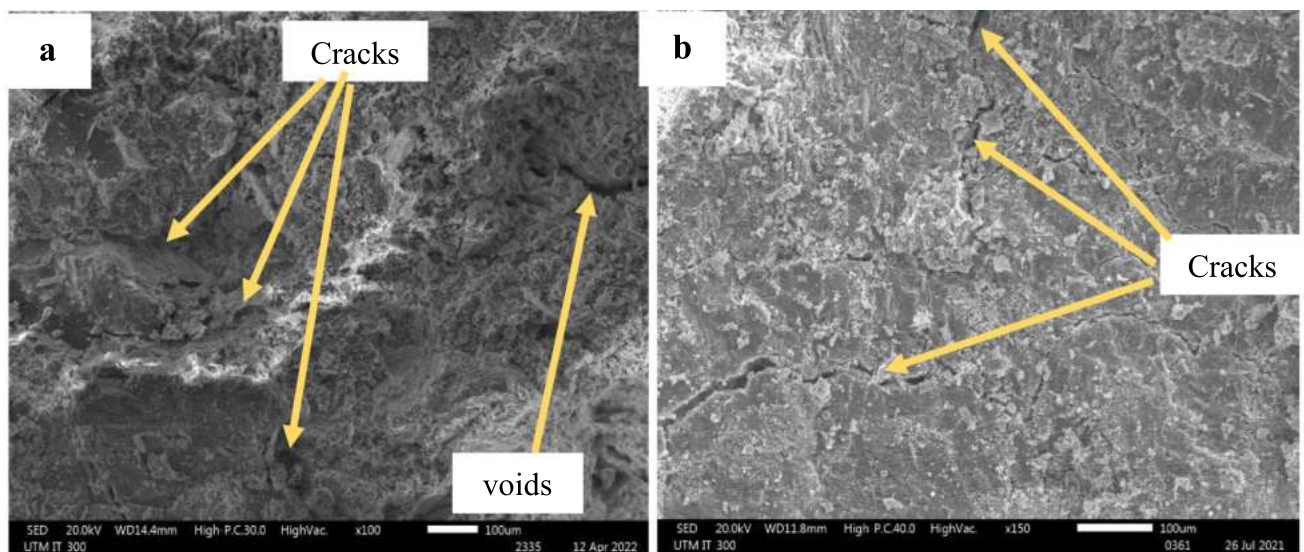**Fig. 15** **a** KFNSC at 400 °C and **b** PNSC at 400 **°C**

Fig. 16 **a** KFNSC at 600 °C and **b** PNSC at 600 °C

This confirms the report of Ogunbode et al. [19], with hemp fibre, at 400 °C and 1-h exposure. However, some voids were observed under the kenaf fibre, as shown in Fig. 15a. These were not thermally induced voids but voids caused by the bridging operation of the kenaf fibre during concrete mixing. In addition, the kenaf fibre partially reduced the compartment of cement paste and aggregates [46]. However, C-S-H had become crystallised in both mixes, which caused the upsurge in the compressive strength observed at this temperature. Also, the transformation of C-S-H gel to crystalline stages enhanced strength more than the preliminary C-S-H gel. Thus, a new crystalline segment with free lime made during cement hydration created a denser microstructure. This was accountable for additional solid volume and bond strength,

which caused a 3–2% and 2% compressive strength shoot-up for KFNSC and PNSC at 400 °C, respectively, above the unheated samples [62]. Also, the same phenomenon played out for the upsurge in split tensile strength at 300 °C for both mixes.

At 600 °C for 1 h (Fig. 16a), KFNSC had become coarser with cracks and voids, while PNSC had also incurred cracks (Fig. 16b). The kenaf fibres have shrunk and frailed, enhancing the microcracks within the matrix. At this temperature and exposure, the portlandite had broken down, given out CaO and water, and the aggregates had transformed, with quartz phase change β–α. The volume of C-S-H gel decreased due to the dehydration of C-S-H, which made both matrices porous. As the temperature increases, pore pressure also
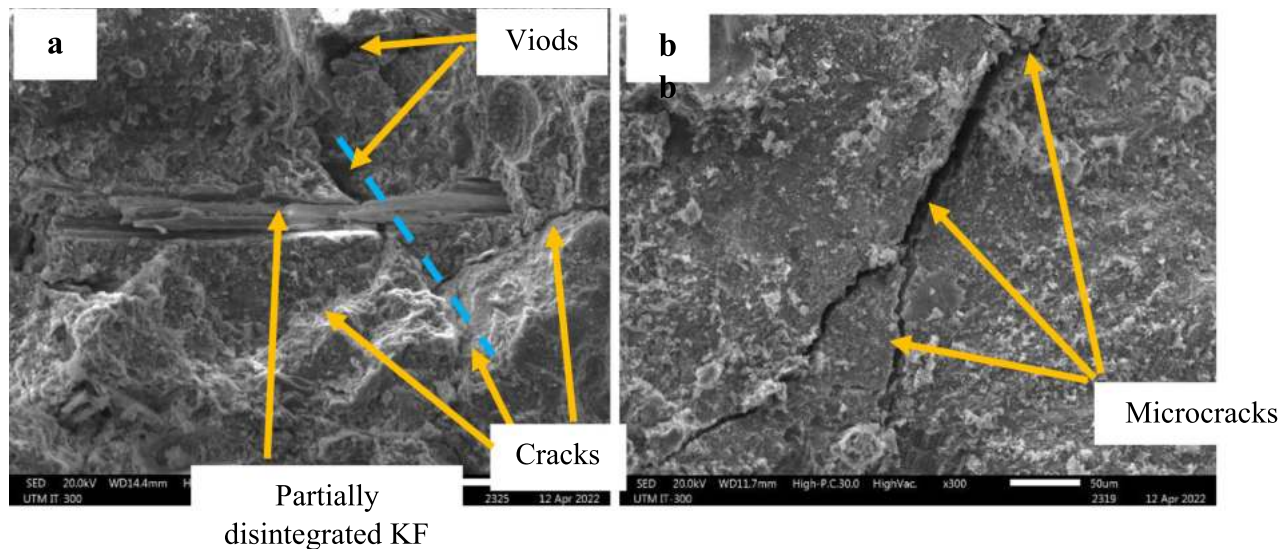
Fig. 17 **a** KFNSC at 800 °C and **b** PNSC at 800 °C

increases. Also, at 800 °C, the second stage of the C-S-H disintegration and creation of β-C2S commenced. The KFNSC sample had degraded and was characterised by some cracks and voids. However, it was surprising to see kenaf fibre remaining in the matrix and not wholly degraded (Fig. 17a). It indicates that kenaf fibre still performs some bridging functions and arrests cracks. The fibre was observed spanning across potential crack lines (Fig. 17a), compared to the PNSC sample, in which the crack network had widened and unabated (Fig. 17b). At 800 °C, there was a noticeable alteration between the permeability of fibrous and non-fibrous samples. The contrasted kenaf fibre (Fig. 17a) allows for free passage and discharge of pore pressure. This could lessen the vapour pressure in the KFNSC mixture bared to elevated temperatures and reduce the risk of concrete spalling. However, explosive spalling is not common in normal-strength concrete [63]. In contrast, this was not the case in the PNSC sample. This report differs from the report by Zhang et al. [14] on Jute fibre as a spalling mitigation strategy.

3.5.3 SEM Results of KFNSC for 2-Hour Temperature Exposure

Figures 18, 19, and 20 reveal the effect of elevated temperatures on the KFHSC for 2 h and the role of the kenaf fibres within the matrix as compared with the control samples.

Figures 18, 19, & 20 depict the SEM images of KFNSC exposed to 400 °C, 600 °C, and 800 °C for 2-h exposure. At 400 °C for 2 h (Fig. 18a), the KFNSC matrix still contained some undegraded kenaf fibre, probably serving as crack arresters. However, these kenaf fibres were shorter than those in Fig. 18a, spanning across the matrix. At this exposure temperature and duration, some crystallised C-S-H was

observed in both matrices (Fig. 18a & b). This was accredited to the slight improvement in the KFNSC compressive strength, having 5% higher than the unheated sample, and PNSC with 100% strength recovery at 300 °C observed at this temperature. Also, the change of C-S-H gel to crystalline stages boosted strength more than the initial C-S-H gel. Thus, a new crystalline segment with free lime made during cement hydration created a denser microstructure [62]. Although not as dense as the 1-h exposure, the 2-h exposure duration made the sample incur some detached pores due to vapour movement and enlarged pore pressure at 450 °C. Unlike the 1-h exposure, C-S-H crystallisation had no notable effect on split and flexural strengths. Some hairline microcracks were spotted on PNSC. However, there were no cracks on KFNSC. This showed the effectiveness of the kenaf fibre in arresting cracks within the matrix. The finding is not different from the report by Mihoub et al. (2020)[17] on Alfa fibre.

At 600 °C, the effect of elevated temperature and exposure duration had begun to take a toll on both matrix materials. There was a speedy volume increase in aggregate due to α-β stage change [61]. The swift expansion in aggregate at around this temperature contradicted the shrinkage of hardened cement paste, leading to severe impairment and cracks at the boundary between aggregates and nearby cement paste. As a result, both matrices experienced cracks and voids (Fig. 19a & b). This was attributed to the ultimate declination of compressive strength at this temperature. At 600 °C and above, for KFNSC and PNSC, the C-S-H phase would have decomposed, and the cement matrix changed into a loose white material that is permeable and feeble. The resultant concrete degradation at this temperature was substantial, as about 50% of strength properties were lost at 600 °C. Finally,
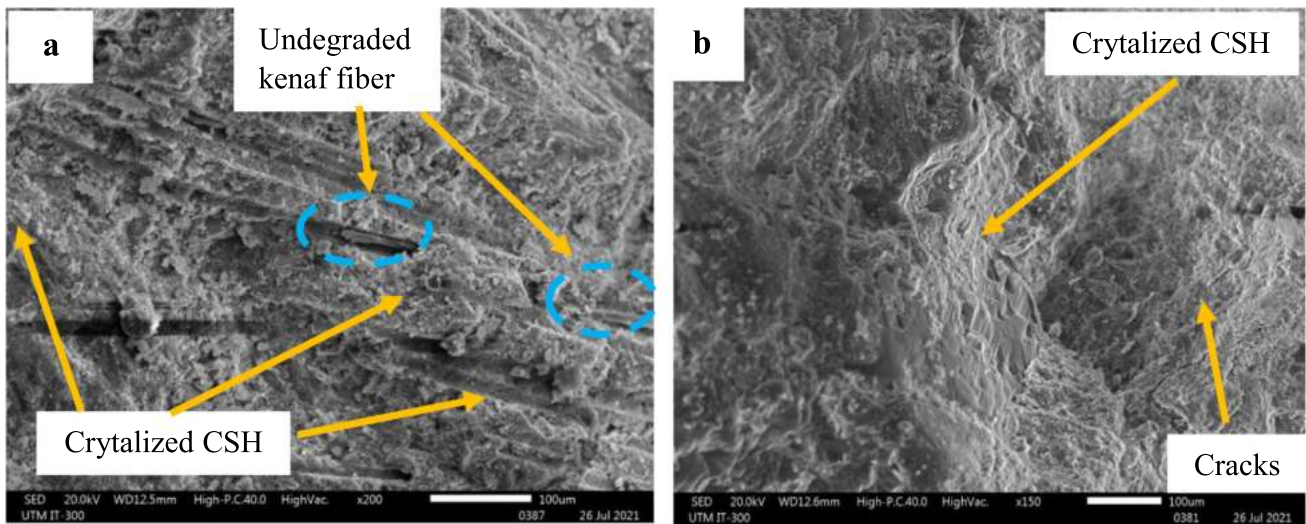
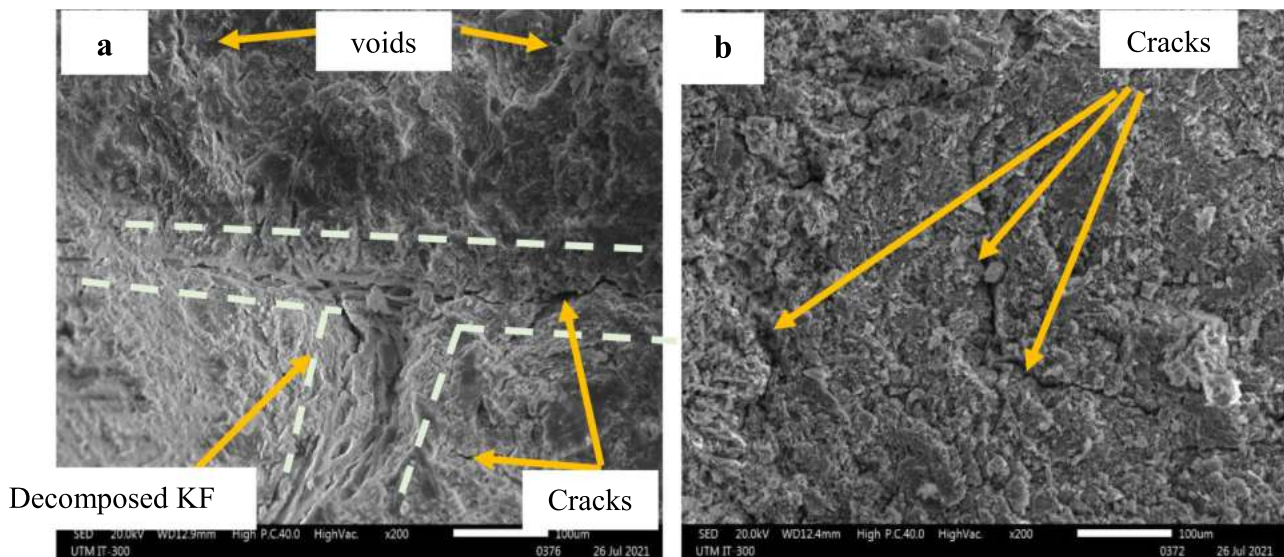**Fig. 18** Micrograph of **a** KFNSC and **b** PNSC at 400 °C

Fig. 19 Micrograph of **a** KFNSC and **b** PNSC at 600 °C

the complete decomposition of kenaf fibre increased cracks within the matrix (Fig. 19a).

Figure 20a reveals the SEM image at 800 ºC. After 2 h, the kenaf fibre had decomposed completely, creating voids and cracks within the matrix. The matrices had completely dehydrated, which is one of the reasons for crack propagation on the samples. The cracks in PNSC had also widened, as shown in Fig. 20b. For KFNSC and PNSC, the complete decomposition of C-S-H is very conspicuous. This temperature is the beginning of the transformation of the matrix into an amorphous structure, engendering many cracks and voids that appeared throughout the concrete samples (Fig. 20a & b). At 800 ºC, C-S-H had deteriorated, and the microstructures of all samples were tremendously damaged. However, the mode of failure of both matrices was satisfactory at this

temperature, and strength retention was between 9 and 15% of their original strength. At this stage, the micrograph of hydration products was characterised by many microcracks and had become amorphous structures because it had lost the crystal structure properties. These findings agree with Zhang et al. [14].

3.5.4 SEM Result of KFNSC for 3-Hour Temperature Exposure

Figures 21, 22, and 23 reveal the effect of elevated temperatures on the KFNSC for 3 h and the role of the kenaf fibres within the matrix compared with the PNSC samples.

The figures showed the SEM images of KFNSC and PNSC exposed to 400 °C, 600 °C, and 800 °C. At 400 °C
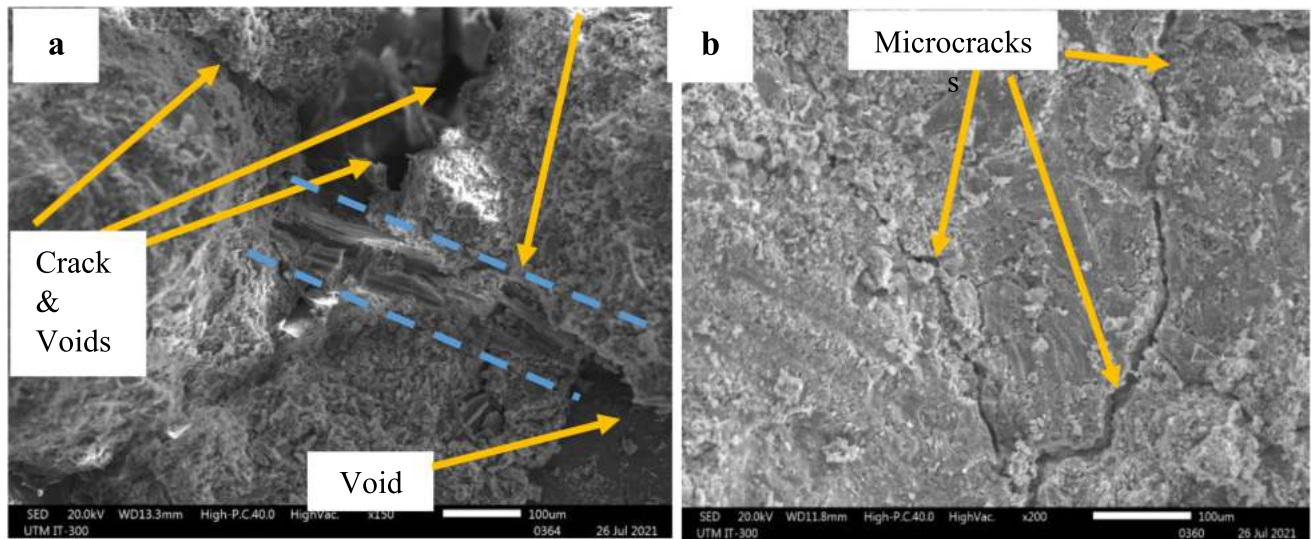
Decomposed KF

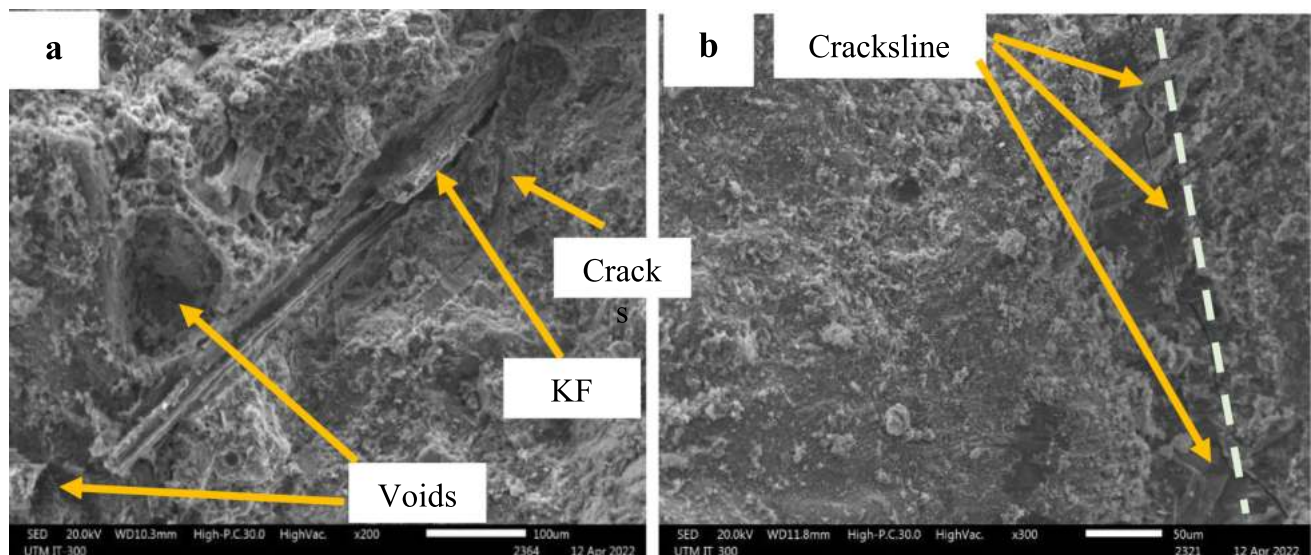Fig. 20 Micrograph **a** KFNSC and **b** PNSC at 800 °C

Fig. 21 Micrograph of **a** KFNSC and **b** PNSC at 400 °C

for 3 h (Fig. 20a), the KFNSC matrix still contained some undegraded kenaf fibre, probably serving as crack arresters. However, these kenaf fibres are shorter than the 2-h exposure (Fig. 18a). At this exposure temperature and duration, very scanty crystallised C-S-H was observed in both matrices (Fig. 21a & b). However, the 3-h exposure impacted the matrices, so KFNSC compressive strength neither declined nor improved. Surprisingly, at this exposure duration, no cracks were observed on KFNSC. In contrast, the PNSC had a long crack line on the cement paste of the matrix (Fig. 21b). This showed how effectively the kenaf fibre performed up to 400 °C for a 3-h duration, which was evident in the mode of failure for KFNSC.

At 600 °C for 3 h, the exposure duration seriously impacted the matrix materials. PNSC was characterised by many cracks and voids, as revealed in Fig. 22b. The KFNSC matrix was also filled with voids created by the pull-out of the kenaf fibre, and some cracks were displayed on the matrix (Fig. 22a). A rapid volume change in aggregate due to α-β stage change occurred [61]. The swift expansion in aggregate at around this temperature contradicted the shrinkage of hardened cement paste, leading to severe damage and cracks at the boundary between aggregates and nearby cement paste. As a result, both matrices experienced cracks and voids (Fig. 22a & b). This was attributed to the practical reduction of compressive strength properties at this temperature. About 50%
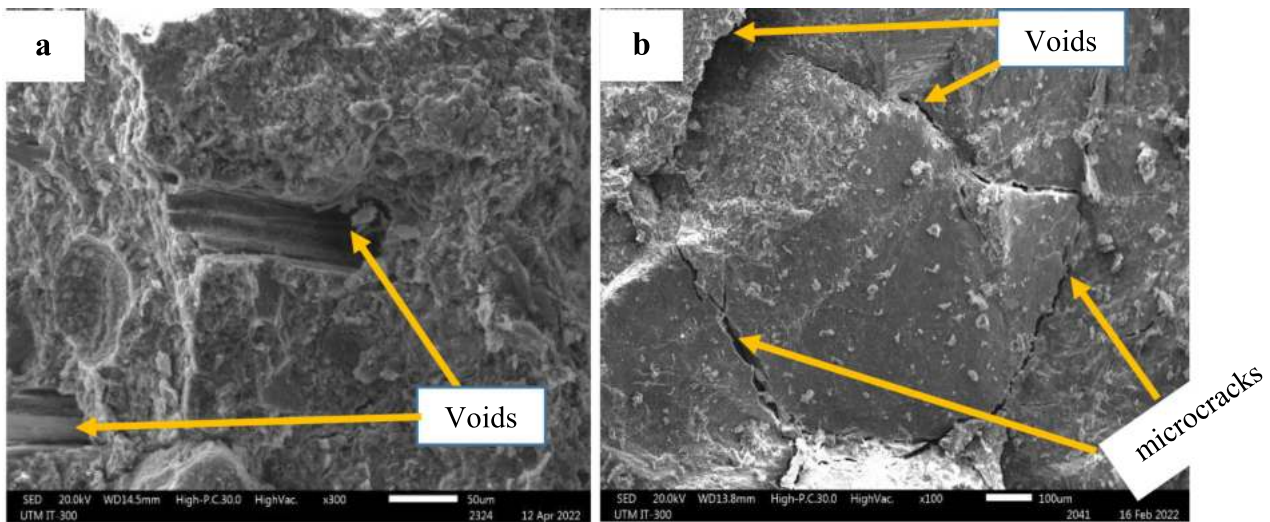
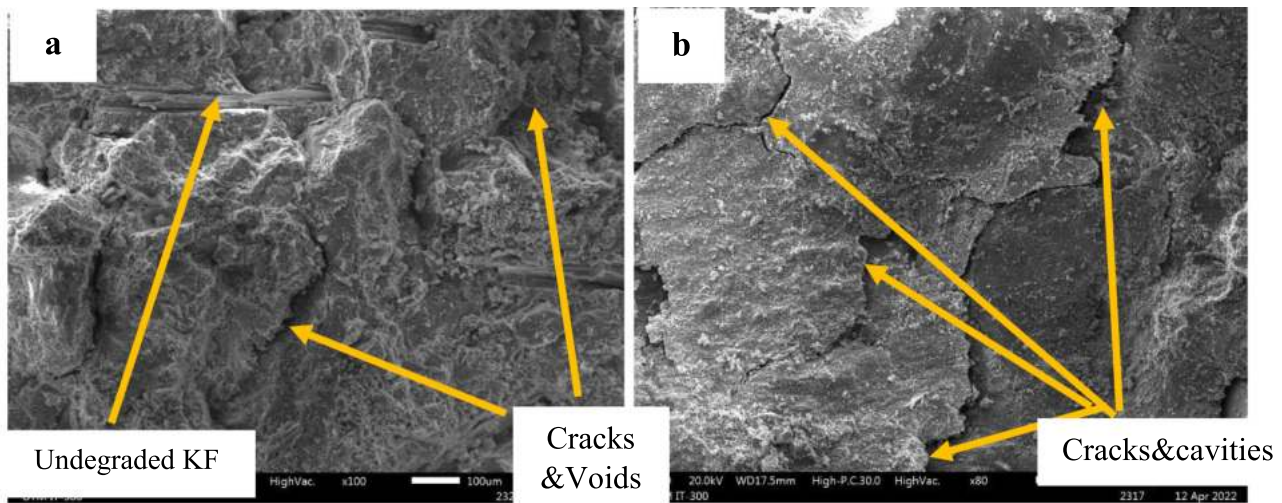**Fig. 22** Micrograph of **a** KFNSC and **b** PNSC at 600 °C

Fig. 23 **a** KFNSC and **b** PNSC at 800 °C

of strength and 11% of weight had been lost. At a temperature higher than this, for KFNSC and PNSC, the C-S-H phase would have broken down, and the cement matrix changed into a loose white material that is very frail and porous. The degradation of the kenaf fibre increased voids and cracks propagation within the matrix (Fig. 22a), consequently creating a passage for pore pressure discharge.

At 800 °C for the 3-h duration, both samples had worsened. The fibres have shrunk and frailed, enhancing the microcracks. The decomposition of C-S-H is very conspicuous. Both matrices had transformed into an amorphous structure at this temperature, engendering many cracks that appeared throughout the concrete samples (Fig. 23a & b). The cracks and cavities were widened due to the exposure duration, which allowed the complete transformation of the

crystal structure to an amorphous form. At 800 °C, C-S-H deteriorated, and the microstructures of all samples were tremendously damaged.

3.6 Prediction Model for KFNSC

The attempt to develop the relationship between the residual compressive strength, temperature, and exposure duration was the reason for the prediction from empirical data, using the response variables (compressive strength) and predictors (elevated temperature, d_0; exposure duration, d_1). Since the optimum kenaf fibre volume and length were used in the research, they were therefore considered constant. Thus, a single GEP-based model for compressive strength for

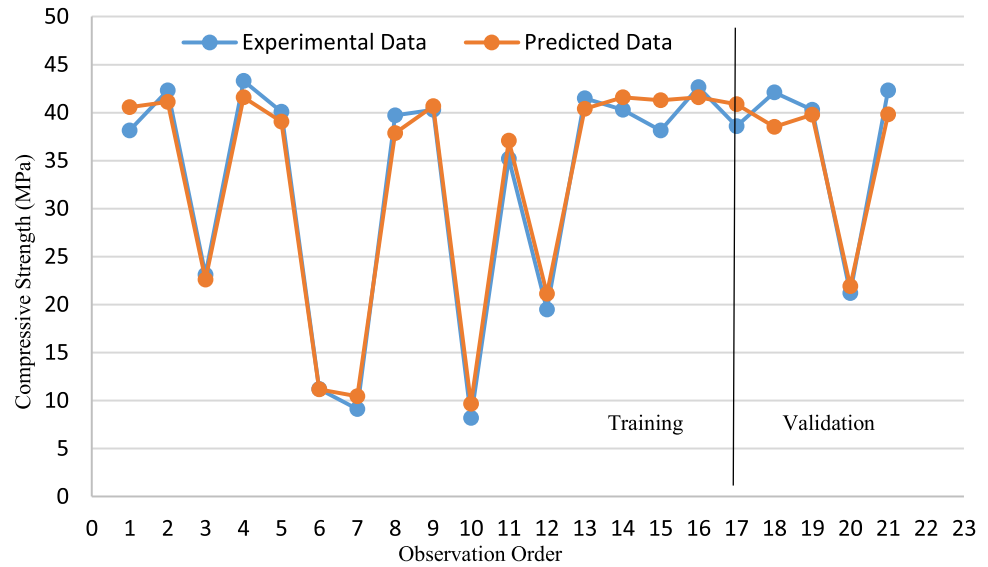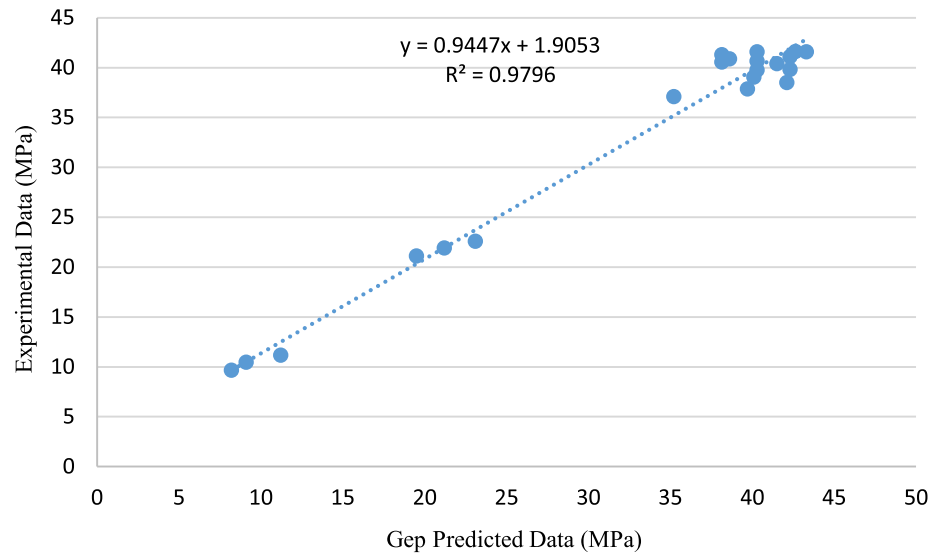**Fig. 24** Curve fittings for the training and validation set for KFNSC

Fig. 25 Scatter plot for KFNSC

KFNSC is presented. This section gives the curve fitting for training and validation, scattered plots, the expression tree, the developed model, and other validation requirements for KFNSC compressive strength prediction presented in Figs. 24, 25, 26, 27. Figure 24 shows the curve fitting for training and validation, with the blue colour for the experimental compressive strength data and the wine colour for the predicted compressive strength GEP data. This is confirmed in Table 7, with minimised errors, a correlation coefficient of 0.99, R^2 of 0.98 for training, a correlation coefficient of 0.947, and R^2 of 0.897 for the validation. The errors in training results were less than the validation results, probably due to a lower data set. Figure 25 shows the correlation between the target (empirical data) and the developed model. Figure 26 shows the impact of elevated temperatures on experimental and predicted data. The model was extracted from ETs

(Fig. 27) and is shown in Eq. 3. The predicted and measured values have a strong correlation according to the GEP model. The GEP model also has prediction ability and generalisation performance, as evidenced by the high R^2 and low error values for testing and confirmation. As a result, the model has demonstrated excellent capability in predicting residual compressive strength of fire-damaged KFNSC. It is shown in Figs. 24 and 25 that the distributions of points are nearly an ideal fit.

3.7 Final developed KFNSC prediction model

$$f_c = \left[\left[\frac{-217.278}{d1} + d0\right]^{1/3} - \left(\frac{d1^{-1} + 2d0}{2}\right)\right]$$

Fig. 26 Scatter plot of experimental data and GEP model data vs high temperature
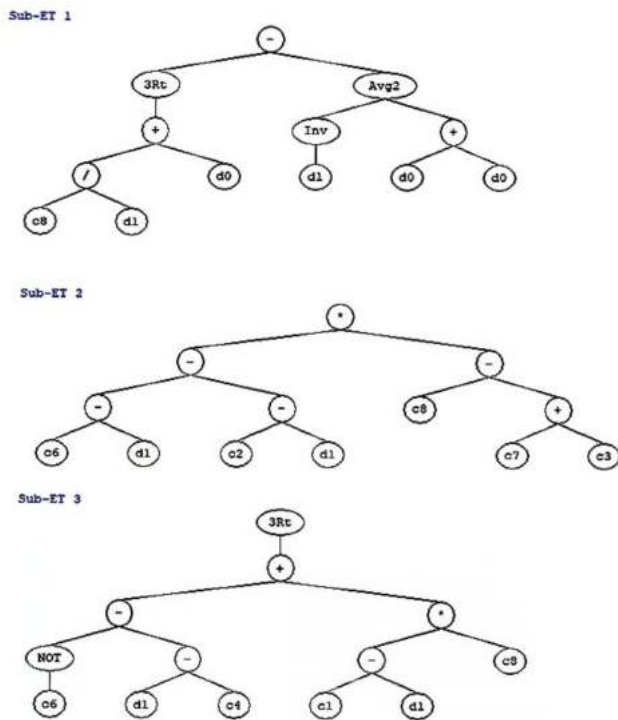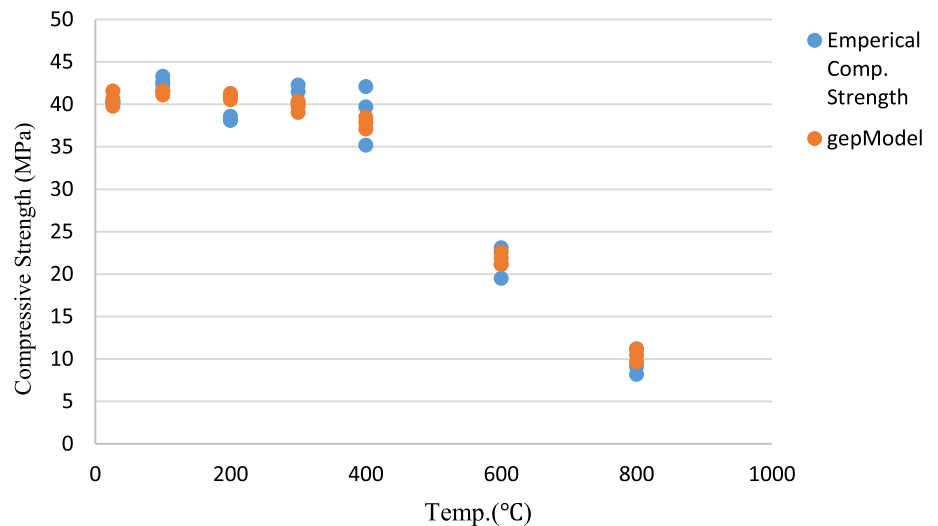

Fig. 27 Expression trees for KFNSC prediction model

$$+ [[(6.353 - \boldsymbol{d}1) - (-0.640 - \boldsymbol{d}1)] \times (3.557)]$$
$$+ [[(-0.647) - (\boldsymbol{d}1 - 535.573)]$$
$$+ ((604.428 - \boldsymbol{d}1) \times 11.972)]^{1/3} \qquad (3)$$

where f_c is the residual compressive strength, $d_0 =$ exposure duration, and the $d_1 =$ temperatures.

4 Conclusion

The research presents experimental reports on the effects of the kenaf fibre and elevated temperatures on concrete composite, assessing the weight loss, UPV, compressive strength, and microstructure of KFNSC. The following conclusion has been drawn:

- Kenaf fibre modification is essential to improve fibre interfacial properties as it reduces the cellulose, hemicellulose, and lignin content on the fibre surface. In addition, treated kenaf fibre showed thermal stability compared with untreated, and its effect was seen in the composite response to varying thermal loads.
- The UPV result of KFNSC and PNSC samples showed soundness till 400 °C. However, KFNSC and PNSC had 72% and 68%, 77% and 72%, 83% and 80% UPV loss at 800 °C for 1, 2, and 3 h, respectively. The KFNSC had a significant loss compared to PNSC due to the pores caused by fibre and concrete material decomposition at higher temperatures and duration.
- Weight loss for both mixes from ambient temperature to 200 °C was mild, almost linearity and stabilised until 300 °C, rising with 5.8% and 5.5% loss at 400 °C. Then, it became substantial at 800 °C for KFNSC with 10.4% and 9.53%, 11.7% and 10.1%, 12.7% and 11.4/% weight loss for 1, 2, and 3 h of KFNSC and PNSC, respectively. Fibre deterioration had little influence on concrete weight loss compared to the complete dehydration of cement paste and decomposition of aggregates at 800 °C.
- Adding kenaf fibre to the concrete composite did not enhance the residual compressive strength of KFNSC. However, as observed in the macrostructure, it played a remarkable role in the bridging mechanism at the lower temperature phase. Also, it topped up its compressive

Table 7 Model statistical fitness for training and validation dataset

GEP 1	R^2	Correl	MAE	RSE	RAE	RRSE	RMSE
Training	0989	0.994	1.273	0.012	0.107	0.107	1.397
Validation	0.897	0.947	1.966	0.104	0.411	0.322	2.265

strength at 300 °C and could still retain 97% of its room temperature strength at 400 °C, while PNSC had an improved strength of 3% higher than its ambient strength. Eventually, KFNSC and PNSC could retain only 800 °C 28% and 34%, 23% and 29%, 20% and 25% of the original (26 °C) compressive strength for 1, 2, and 3 h, respectively.

- For KFNSC microstructure, for the 1-h heating at up to 800 °C, the kenaf fibre still provided a bridging mechanism, mitigating crack extension and thermal incompatibility of the aggregate and cement paste within the matrix. For a 2-h heating period, this mechanism did not change till 400 °C before the coarsening of both matrices, which is the development of pore structures due to the exposure temperature and duration. On the other hand, during the 3-h heating periods, degradation of the concrete materials commenced at 400 °C and continued till 800 °C with massive worsening effects on both matrices. For KFNSC, the kenaf fibre played a unique role in cracks and pore pressure mitigation up to 600 °C for 1, 2, and 3 exposure durations, which was a considerable advantage over PNSC. However, the decomposition of C-S-H and aggregates, coupled with kenaf fibre disintegration, caused total deterioration of KFNSC, which was reflected in strength losses and weight losses.

- The performance of the kenaf fibre in normal-strength concrete has been beneficial and looks promising in alleviating pore pressure build-up in heated high-strength concrete. The morphological images were appropriately well matched with strength properties. It revealed that the strength shoot-up at 400 °C was due to the crystallisation of C-S-H, forming more incredible bonds within the mixes. Also, the remaining undisintegrated fibres reduced crack reduction. Also, at 800 °C, the microstructures became porous due to the amorphous state and the microcracks. Finally, the decomposition of cement paste, aggregate, and fibre led to the complete breakdown of the cement paste–aggregate–fibre bond.

- For the GEP-based model, comparing the predicted residual numerical data and the empirical data, it can be concluded that the model has high accuracy and reliability.

It is recommended that research on the fire performance of high-strength concrete containing a hybrid of steel and kenaf fibres be encouraged to explore the kenaf fibre potential in pore pressure reduction and mitigation of thermal incompatibility of aggregates and hardened cement paste under thermal load. Also, fibre distribution is one of the reasons for reduced biofibre-reinforced concrete strength. Therefore, a uniform distribution mechanism of short-discrete fibre should be developed.

Declarations

Conflict of interest The authors declare that they have no known competing financial interests or personal.

References

1. Aluko, O.G.; Yatim, J.M.; Kadir, M.A.A.; Yahya, K.: A review of properties of bio-fibrous concrete exposed to elevated temperatures. Constr. Build. Mater. **260**, 119671 (2020). https://doi.org/10.1016/j.conbuildmat.2020.119671
2. Ogunbode Ezekiel Babatunde, CREEP AND SHRINKAGE PERFORMANCE OF KENAF BIO FIBROUS, (2017)
3. Jones, D.; Ormondroyd, G.O.; Curling, S.F.; Popescu, C.M.; Popescu, M.C.: Chemical compositions of natural fibres. Adv. High Strength Nat. Fibre Compos. Constr. (2017). https://doi.org/10.1016/B978-0-08-100411-1.00002-9
4. Ramesh, M.: Kenaf (*Hibiscus cannabinus* L.) fibre based biomaterials: A review on processing and properties. Prog. Mater. Sci. **78–79**, 1–92 (2016). https://doi.org/10.1016/j.pmatsci.2015.11.001
5. Novák, J.; Kohoutková, A.: Fire response of hybrid fiber reinforced concrete to high temperature. Procedia Eng. **172**, 784–790 (2017). https://doi.org/10.1016/j.proeng.2017.02.123
6. Kodur, V.: Properties of concrete at elevated temperatures. ISRN Civ. Eng. **2014**, 1–15 (2014). https://doi.org/10.1155/2014/468510
7. Memon, S.A.; Shah, S.F.A.; Khushnood, R.A.; Baloch, W.L.: Durability of sustainable concrete subjected to elevated temperature – a review. Constr. Build. Mater. **199**, 435–455 (2019). https://doi.org/10.1016/j.conbuildmat.2018.12.040
8. Ozawa, M.; Morimoto, H.: Effects of various fibres on high-temperature spalling in high-performance concrete. Constr. Build. Mater. **71**, 83–92 (2014). https://doi.org/10.1016/j.conbuildmat.2014.07.068
9. Jin, L.; Zhang, R.; Dou, G.; Du, X.: Fire resistance of steel fiber reinforced concrete beams after low-velocity impact loading. Fire Saf. J. **98**, 24–37 (2018). https://doi.org/10.1016/j.firesaf.2018.04.003
10. Ding, Y.; Zhang, C.; Cao, M.; Zhang, Y.; Azevedo, C.: Influence of different fibers on the change of pore pressure of self-consolidating concrete exposed to fire. Constr. Build. Mater. **113**, 456–469 (2016). https://doi.org/10.1016/j.conbuildmat.2016.03.070

11. Choumanidis, D.; Badogiannis, E.; Nomikos, P.; Sofianos, A.: The effect of different fibres on the flexural behaviour of concrete exposed to normal and elevated temperatures. Constr. Build. Mater. **129**, 266–277 (2016). https://doi.org/10.1016/j.conbuildmat.2016.10.089

12. Sadrinejad, I.; Madandoust, R.; Ranjbar, M.M.: The mechanical and durability properties of concrete containing hybrid synthetic fibers. Constr. Build. Mater. (2018). https://doi.org/10.1016/j.conbuildmat.2018.05.145

13. Ozawa, M.; Sato, R.; Yoon, M.-H.; Rokugo, K.; Kim, G.-Y.; Choe, G.-C.: Thermal properties of jute fiber concrete at high temperature. J. Struct. Fire Eng. **7**, 182–192 (2017). https://doi.org/10.1108/jsfe-09-2016-017

14. Zhang, D.; Tan, K.H.; Dasari, A.; Weng, Y.: Effect of natural fibers on thermal spalling resistance of ultra-high performance concrete. Cem. Concr. Compos. **109**, 103512 (2020). https://doi.org/10.1016/j.cemconcomp.2020.103512

15. Netinger Grubeša, I.; Marković, B.; Gojević, A.; Brdarić, J.: Effect of hemp fibers on fire resistance of concrete. Constr. Build. Mater. **184**, 473–484 (2018). https://doi.org/10.1016/j.conbuildmat.2018.07.014

16. Juradin, S.; Vranješ, L.K.; Jozić, D.; Boko, I.: Post-fire mechanical properties of concrete reinforced with spanish broom fibers. J. Compos. Sci. **5**, 1–17 (2021). https://doi.org/10.3390/jcs5100265

17. Imane Mihoub, S.M.; Khelifa, M.R.: Impact of elevated temperature on the properties of concretes reinforced. Civ. Environ. Eng. Reports. **30**, 161–185 (2020). https://doi.org/10.2478/ceer-2020-0038

18. Babalola, O.E.; Awoyera, P.O.; Le, D.-H.; Bendezú Romero, L.M.: A review of residual strength properties of normal and high strength concrete exposed to elevated temperatures: impact of materials modification on behaviour of concrete composite. Constr. Build. Mater. **296**, 123448 (2021). https://doi.org/10.1016/j.conbuildmat.2021.123448

19. Babatunde, O.E.; Yatim, J.M.; Razavi, M.; Yunus, I.M.; Azzmi, N.M.: Experimental study of Kenaf bio fibrous concrete. Composites **24**, 3922–3927 (2018). https://doi.org/10.1166/asl.2018.11512

20. Elsaid, A.; Dawood, M.; Seracino, R.; Bobko, C.: Mechanical properties of kenaf fiber reinforced concrete. Constr. Build. Mater. **25**, 1991–2001 (2011). https://doi.org/10.1016/j.conbuildmat.2010.11.052

21. Edeerozey, A.M.M.; Akil, H.M.; Azhar, A.B.; Ariffin, M.I.Z.: Chemical modification of kenaf fibers. Mater. Lett. **61**, 2023–2025 (2007). https://doi.org/10.1016/j.matlet.2006.08.006

22. Akil, H.M.; Omar, M.F.; Mazuki, A.A.M.; Safiee, S.; Ishak, Z.A.M.; Abu Bakar, A.: Kenaf fiber reinforced composites: A review. Mater. Des. **32**, 4107–4121 (2011). https://doi.org/10.1016/j.matdes.2011.04.008

23. Kodur, V.K.R.; Raut, N.K.; Mao, X.Y.; Khaliq, W.: Simplified approach for evaluating residual strength of fire-exposed reinforced concrete columns. Mater. Struct. Constr. **46**, 2059–2075 (2013). https://doi.org/10.1617/s11527-013-0036-2

24. Ferreira, C.: Gene expression programming in problem solving. Soft Comput. Ind. (2002). https://doi.org/10.1007/978-1-4471-0123-9_54

25. Ashteyat, A.; Obaidat, Y.T.; Murad, Y.Z.; Haddad, R.: Compressive strength prediction of lightweight short columns at elevated temperature using gene expression programing and artificial neural network. J. Civ. Eng. Manag. **26**, 189–199 (2020). https://doi.org/10.3846/jcem.2020.11931

26. Tanyildizi, H.; Çevik, A.: Modeling mechanical performance of lightweight concrete containing silica fume exposed to high temperature using genetic programming. Constr. Build. Mater. **24**, 2612–2618 (2010). https://doi.org/10.1016/j.conbuildmat.2010.05.001

27. Sonebi, M.; Cevik, A.: Genetic programming based formulation for fresh and hardened properties of self-compacting concrete containing pulverised fuel ash. Constr. Build. Mater. **23**, 2614–2622 (2009). https://doi.org/10.1016/j.conbuildmat.2009.02.012

28. Nematzadeh, M.; Shahmansouri, A.A.; Zabihi, R.: Innovative models for predicting post-fire bond behavior of steel rebar embedded in steel fiber reinforced rubberized concrete using soft computing methods. Structures. **31**, 1141–1162 (2021). https://doi.org/10.1016/j.istruc.2021.02.015

29. Akil, H.M.; Omar, M.F.; Mazuki, A.A.M.; Safiee, S.; Ishak, Z.A.M.; Bakar, A.A.: Kenaf fiber reinforced composites: a review Kenaf fiber reinforced composites: a review. Mater. Des. **32**, 4107–4121 (2011). https://doi.org/10.1016/j.matdes.2011.04.008

30. Mahjoub, R.; Mohamad, J.; Rahman, A.; Sam, M.; Hamid, S.: Tensile properties of kenaf fiber due to various conditions of chemical fiber surface modifications. Constr. Build. Mater. **55**, 103–113 (2014). https://doi.org/10.1016/j.conbuildmat.2014.01.036

31. Bashah, N.B.M.K.: Properties Of Kenaf Fibrous Pulverised Fuel Ash Concrete, Universiti Teknologi Malaysia (2018)

32. Lam, T.F.; Yatim, J.M.: Mechanical properties of kenaf fiber reinforced concrete with different fiber content and fiber length. J. Asian Concr. Fed. **1**, 11 (2015). https://doi.org/10.18702/acf.2015.09.1.11

33. BS-EN-14889-2, Fibres for concrete - Part 2: Polymer fibres. Definitions, specifications and conformity, Bsi. 3 (2006) 30

34. Norul Izani, M.A.; Paridah, M.T.; Anwar, U.M.K.; Mohd Nor, M.Y.; H'Ng, P.S.: Effects of fiber treatment on morphology, tensile and thermogravimetric analysis of oil palm empty fruit bunches fibers. Compos. Part B Eng. **45**, 1251–1257 (2013). https://doi.org/10.1016/j.compositesb.2012.07.027

35. ASTM E119-16a, ASTM E119: Standard Test Methods for Fire Tests of Building Construction and Materials, ASTM Int. West Conshohocken, PA. 552 (2016). https://doi.org/10.1520/E0119-14

36. Khaliq, W.: Taimur, Mechanical and physical response of recycled aggregates high-strength concrete at elevated temperatures. Fire Saf. J. **96**, 203–214 (2018). https://doi.org/10.1016/j.firesaf.2018.01.009

37. ASTM-C150, ASTM C150, 04 (2002) 1–7

38. BS EN 12350-2, Testing fresh concrete, Part 2: Slump-test. BSI, (2009)

39. ISO 834-12, International Standard: Fire resistance tests — Elements of building construction, (2012). https://www.sis.se/std-915507

40. Schneider, U.; Schwesinger, P.; Debicki, G.S.; Diederichs, U.; Felicetti, R.; Franssen, J.M.; Jumppanen, U.M.; Khoury, G.A.; Millard, A.A.; Morris, W.A.; Phan, L.: Recommendation of RILEM TC 200-HTC: Mechanical concrete properties at high temperatures-modelling and application : Part 11: Relaxation. Mater. Struct. Constr. **40**, 449–458 (2007). https://doi.org/10.1617/s11527-006-9203-z

41. Li, Q.; Wang, M.; Sun, H.; Yu, G.: Effect of heating rate on the free expansion deformation of concrete during the heating process. J. Build. Eng. **34**, 101896 (2021). https://doi.org/10.1016/j.jobe.2020.101896

42. Chan, Y.N.; Peng, G.F.; Anson, M.: Residual strength and pore structure of high-strength concrete and normal strength concrete after exposure to high temperatures. Cem. Concr. Compos. **21**, 23–27 (1999). https://doi.org/10.1016/S0958-9465(98)00034-1

43. Peng, G.F.; Bian, S.H.; Guo, Z.Q.; Zhao, J.; Peng, X.L.; Jiang, Y.C.: Effect of thermal shock due to rapid cooling on residual mechanical properties of fiber concrete exposed to high temperatures. Constr. Build. Mater. **22**, 948–955 (2008). https://doi.org/10.1016/j.conbuildmat.2006.12.002

44. Phanl, L.T.; Lawson, J.R.; David, F.L.: Characteristics, spalling, and residual properties of high performance concrete. Mater. Struct. Constr. **34**, 83–91 (2001)

45. BS EN 12350-3, Testing hardened concrete:Compressive strength of test specimens. BSI, (2009)

46. Neville, J.B.: Concrete Technology, 2nd edn. Longman Group UK Limited, London (2010)

47. Zheng, W.; Li, H.; Wang, Y.: Compressive stress – strain relationship of steel fiber-reinforced reactive powder concrete after exposure to elevated temperatures. Constr. Build. Mater. **35**, 931–940 (2012). https://doi.org/10.1016/j.conbuildmat.2012.05.031

48. Awal, A.S.M.A.; Shehu, I.A.: Performance evaluation of concrete containing high volume palm oil fuel ash exposed to elevated temperature. Constr. Build. Mater. **76**, 214–220 (2015). https://doi.org/10.1016/j.conbuildmat.2014.12.001

49. Hossein Mohammadhosseini, J.M.Y.: Microstructure and residual properties of green concrete composites incorporating waste carpet fibers and palm oil fuel ash at elevated temperatures. J. Clean. Prod. J. **144**, 8–21 (2017). https://doi.org/10.1016/j.jclepro.2016.12.168

50. Awal, A.S.M.A.; Shehu, I.A.; Ismail, M.: Effect of cooling regime on the residual performance of high-volume palm oil fuel ash concrete exposed to high temperatures. Constr. Build. Mater. **98**, 875–883 (2015). https://doi.org/10.1016/j.conbuildmat.2015.09.001

51. Demirel, B.; Keleştemur, O.: Effect of elevated temperature on the mechanical properties of concrete produced with finely ground pumice and silica fume. Fire Saf. J. **45**, 385–391 (2010). https://doi.org/10.1016/j.firesaf.2010.08.002

52. Yüksel, S.; Siddique, R.; Özkan, Ö.: Influence of high temperature on the properties of concretes made with industrial by-products as fine aggregate replacement. Constr. Build. Mater. **25**, 967–972 (2011). https://doi.org/10.1016/j.conbuildmat.2010.06.085

53. Guo, Y.C.; Zhang, J.H.; Chen, G.M.; Xie, Z.H.: Compressive behaviour of concrete structures incorporating recycled concrete aggregates, rubber crumb and reinforced with steel fibre, subjected to elevated temperatures. J. Clean. Prod. **72**, 193–203 (2014). https://doi.org/10.1016/j.jclepro.2014.02.036

54. Arioz, O.: Effects of elevated temperatures on properties of concrete. Fire Saf. J. **42**, 516–522 (2007). https://doi.org/10.1016/j.firesaf.2007.01.003

55. Afshoon, I.; Sharifi, Y.: Utilization of micro copper slag in SCC subjected to high temperature. J. Build. Eng. **29**, 101128 (2020). https://doi.org/10.1016/j.jobe.2019.101128

56. Khoury, G.A.: Compressive strength of concrete at high temperatures: A reassessment. Mag. Concr. Res. **44**, 291–309 (1992). https://doi.org/10.1680/macr.1992.44.161.291

57. Wang, C.; Chen, X.; Wei, X.; Wang, R.: Can nanosilica sol prevent oil well cement from strength retrogression under high temperature? Constr. Build. Mater. **144**, 574–585 (2017). https://doi.org/10.1016/j.conbuildmat.2017.03.221

58. Mohamedbhai, G.T.G.: Effect of exposure time and rates of heating and cooling on residual strength of heated concrete. Mag. Concr. Res. **38**, 151–158 (1986). https://doi.org/10.1680/macr.1986.38.136.151

59. Ma, Q.; Guo, R.; Zhao, Z.; Lin, Z.; He, K.: Mechanical properties of concrete at high temperature-A review. Constr. Build. Mater. **93**, 371–383 (2015). https://doi.org/10.1016/j.conbuildmat.2015.05.131

60. Fernandes, B.; Gil, A.M.; Bolina, F.L.; Tutikian, B.F.: Microstructure of concrete subjected to elevated temperatures: physico-chemical changes and analysis techniques. Rev. IBRACON Estruturas e Mater. **10**, 838–863 (2017). https://doi.org/10.1590/s1983-41952017000400004

61. Hager, I.: Behaviour of cement concrete at high temperature. Bull. Polish Acad. Sci. Tech. Sci. **61**, 145–154 (2013). https://doi.org/10.2478/bpasts-2013-0013

62. Al-jabri, K.; Shoukry, H.: Use of nano-structured waste materials for improving mechanical, physical and structural properties of cement mortar. Constr. Build. Mater. **73**, 636–644 (2014). https://doi.org/10.1016/j.conbuildmat.2014.10.004

63. Peng, G.F.; Jiang, Y.C.; Li, B.H.; Zhang, J.; Shi, Y.X.: Effect of high temperature on normal-strength high-performance concrete. Mater. Res. Innov. **18**, S2290–S2293 (2014). https://doi.org/10.1179/1432891714Z.000000000414